
Autocomp: LLM-Driven Code Optimization for Tensor Accelerators

Charles Hong Sahil Bhatia Alvin Cheung Yakun Sophia Shao

UC Berkeley

{charleshong, sahilbhatia, akcheung, ysshao}@berkeley.edu

Abstract

Hardware accelerators, especially those designed for tensor processing, have become ubiquitous in today’s computing landscape. However, even with significant efforts in building compilers, programming these tensor accelerators remains challenging, leaving much of their potential underutilized. Recently, large language models (LLMs), trained on large amounts of code, have shown significant promise in code generation and optimization tasks, but generating low-resource languages like specialized tensor accelerator code still poses a significant challenge. We tackle this challenge with Autocomp, an approach that empowers accelerator programmers to leverage domain knowledge and hardware feedback to optimize code via an automated LLM-driven search. We accomplish this by: 1) formulating each optimization pass as a structured two-phase prompt, divided into planning and code generation phases, 2) inserting domain knowledge during planning via a concise and adaptable optimization menu, and 3) integrating correctness and performance metrics from hardware as feedback at each search iteration. Across three categories of representative workloads and two different accelerators, we demonstrate that Autocomp-optimized code runs $5.6\times$ (GEMM) and $2.7\times$ (convolution) faster than the vendor-provided library, and outperforms expert-level hand-tuned code by $1.4\times$ (GEMM), $1.1\times$ (convolution), and $1.3\times$ (fine-grained linear algebra). Additionally, we demonstrate that optimization schedules generated from Autocomp can be reused across similar tensor operations, improving speedups by up to 24% under a fixed sample budget.

1 Introduction

Hardware accelerators [43, 29] have become a critical driving force for the recent breakthroughs [32, 18, 19, 59, 44] in machine learning. They provide hundred-fold improvements in performance and energy efficiency in running deep neural networks (DNNs), and this has led to an increasing number of accelerators for tensor processing in recent years [29, 46, 42, 34, 27, 13, 6, 8]. However, extracting that performance requires writing high-performance accelerator code, which is time consuming and requires a deep understanding of the underlying hardware.

To address this challenge, various compilers and domain-specific languages (DSLs) have appeared. For deep learning applications, compilers such as XLA, TVM, and Triton generate high-performance code, but they only support a few hardware backends, particularly CPUs and GPUs [45, 7]. Unfortunately, adapting compilers and DSLs to new hardware platforms with vendor-specific instruction set architectures (ISAs) and implementation-specific dataflow patterns requires significant engineering effort. In fact, software alone comprises 40-50% of the development cost for new hardware [58, 54, 23], even before considering the effort needed for end users to write and debug software for a newly developed chip. Prior work in DSLs like Halide and Exo [50, 26] targets accelerators by providing primitives that make it easier to express tensor computation, but the onus of optimizing code written in such DSLs still lies on the accelerator programmer.

Even once a compiler exists, generating performant code runs into the classical “scheduling” problem, i.e., deciding which optimizations to apply and in what order. For general-purpose backends (CPUs and GPUs), these passes have been iteratively developed and refined over many years through a combination of experts and auto-tuning frameworks. Recent work has gone further in exploring data-driven approaches such as supervised learning [66] and reinforcement learning [9], and even LLM training [10] to tackle the combinatorial explosion of pass sequences. While these data-driven approaches have shown promise, they depend on vast amounts of performance data to train, which is painfully scarce for domain-specific hardware accelerators.

In this paper, we present Autocomp, which solves the problems with prior approaches with an iterative LLM-guided search framework to optimize accelerator code. Unlike previous compilers, Autocomp can adapt to new hardware platforms and ISAs by simply changing prompts. Unlike existing tensor DSLs, Autocomp automatically generates optimized code without manual tuning. And unlike data-driven approaches targeting CPUs and GPUs, Autocomp requires no model training, instead leveraging LLM in-context reasoning and pretrained knowledge of common optimizations.

In each iteration, Autocomp first *plans* by choosing an optimization from a predefined menu, i.e., a list of common hardware accelerator optimizations like tiling and unrolling, then *applies* the optimization to generate optimized DSL code. The generated candidates are validated for correctness and benchmarked on the accelerator to collect performance metrics, providing feedback for the next iteration of search. By encoding DSL syntax, optimization rules, and performance feedback concisely in a prompt, Autocomp can guide the LLM to generate optimized code to run on the target accelerator.

In our evaluation, we apply Autocomp to two representative low-resource accelerators and generate code that runs $5.6\times$ (GEMM) and $2.7\times$ (convolution) faster than the vendor-provided library. Furthermore, it outperforms expert-level hand-tuned code by $1.4\times$ (GEMM), $1.1\times$ (convolution), and $1.3\times$ (fine-grained linear algebra), surpassing the prior best known implementations with less human effort. Moreover, we show that Autocomp’s schedules can be reused as guidance when scheduling similar tensor operations, alleviating the cost of scheduling new code and delivering up to 24% greater speedups under a fixed sample budget.

In summary, we make the following contributions in this paper:

1. We present Autocomp, the first LLM-driven code optimization approach for low-resource tensor accelerator code generation.
2. Autocomp incorporates domain knowledge, hardware feedback on correctness and performance, and novel strategies for response diversity to automatically generate performant code.
3. Our generated implementations significantly outperform hand-optimized code written by experts across a wide range of workloads and across different tensor accelerators.
4. We illustrate that schedules generated by Autocomp can be reused to optimize similar tensor operations, reducing search cost and demonstrating the *a posteriori* usefulness of Autocomp-generated schedules beyond pure performance.

2 Background

2.1 Code Optimization for Tensor Accelerators

Programming tensor accelerators differs greatly from programming general-purpose CPUs. Tensor accelerators, depicted in Fig. 1, generally focus on the efficient execution of fixed-size (e.g., 16×16) matrix multiplication instructions, as shown in Fig. 2. Rather than trying to reduce the number or type of these instructions, which is often fixed, software optimization focuses on other aspects, such as:

- Minimizing data movement between main memory and smaller accelerator-local memories (in Fig. 1, the scratchpad and accumulator).
- Setting configuration state for computation and data movement.
- Scheduling or reordering operations to maximally overlap computation and data movement.

Code transformations that enable these optimizations range from low-level changes like arithmetic simplification or instruction selection, to higher-level changes like loop tiling, hoisting (Fig. 3), or software pipelining (Fig. 4). These high-level changes, while improving performance, require

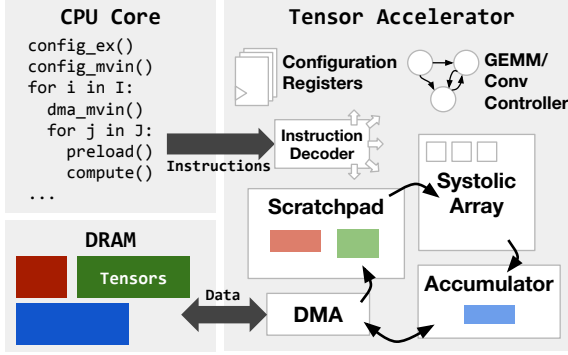


Figure 1: Architecture and dataflow of a tensor accelerator system. Note that data movement is handled explicitly via accelerator direct memory access (DMA) instructions. GEMM/conv controllers refer to on-chip hardware implementations of matrix multiplications and convolutions, used as baselines in Sec. 4.

```

1 // Unoptimized
2 for (int i = 0; i < 8; i++) {
3     for (int j = 0; j < 32; j++) {
4         for (int k = 0; k < 8; k++) {
5             config_mvin(128); // A's stride is 128
6             dma_mvin(A[i*16][k*16], spad_addr_1);
7             config_mvin(256); // B's stride is 256
8             dma_mvin(B[k*16][j*16], spad_addr_2);
9
10 // Optimized
11 config_mvin(128);
12 config_mvin_2(256);
13 for (int i = 0; i < 8; i++) {
14     for (int j = 0; j < 32; j++) {
15         for (int k = 0; k < 8; k++) {
16             dma_mvin(A[i*16][k*16], spad_addr_1);
17             dma_mvin_2(B[k*16][j*16], spad_addr_2);

```

Figure 3: Example of hoisting accelerator configuration instructions, which can block execution. In this case the accelerator supports multiple direct memory access (DMA) load instructions, each with its own configuration state.

loop nests, pointers, and indices to be modified in multiple locations, making them challenging to implement, especially in a low-resource DSL.

Prior work has explored some of this optimization space. For example, performance models like Timeloop [48], MAESTRO [33], and TeAAL [39] use high-level hardware architectural models and software abstractions to represent tensor accelerators and their workloads. Much recent work has sought to automatically explore this space, using methods such as machine learning [21, 25, 53, 20], linear programming [24], black-box optimization [30, 65, 52], and reinforcement learning [64]. While these abstractions capture some aspects of tensor accelerator code optimization, in particular the amount of data movement, they neglect other implementation-specific and instruction-level optimizations. In this work, LLM code generation allows us to directly rewrite accelerator code, expanding the search to include all potential axes of optimization.

2.2 LLM-Based Code Optimization

LLMs have been used in various code-related tasks [5, 41, 2]. For code optimization, several works have utilized evolutionary approaches that take advantage of LLMs' ability to apply novel mutations to code [36, 4, 38, 37, 16, 51]. Others have used methods like in-context learning and retrieval-augmented generation (RAG) to transfer knowledge from a library of previously known optimizations to the current problem [61, 1]. Still others have collected large datasets of performance examples

```

1 // CPU code
2 for (int i = 0; i < N; i++) {
3     for (int j = 0; j < N; j++) {
4         C[i][j] = 0;
5         for (int k = 0; k < N; k++) {
6             C[i][j] += A[i][k] * B[k][j];
7         }
8     }
9 }
10 // Accelerator code
11 for (int ii = 0; ii < N; ii += T) {
12     for (int jj = 0; jj < N; jj += T) {
13         zero_accumulator(acc_addr+...);
14         for (int kk = 0; kk < N; kk += T) {
15             dma_mvin(A[ii*T][kk*T], A_spad_addr);
16             dma_mvin(B[kk*T][jj*T], B_spad_addr);
17             for (int i = 0; i < T; i+=16) {
18                 for (int j = 0; j < T; j+=16) {
19                     for (int k = 0; k < T; k+=16) {
20                         compute(A_spad_addr+..., B_spad_addr+..., acc_addr+...);}}
21         }
22         dma_mvout(acc_addr, C[ii*T][jj*T]);
23     }
24 }

```

Figure 2: Comparison of general-purpose CPU code and tensor accelerator code for matrix multiplication.

```

1 // Unoptimized
2 for (int k = 0; k < 8; k++) {
3     for (int i = 0; i < 32; i++) {
4         dma_mvin(A[i*16][k*64], spad_addr);
5         for (int k_i = 0; k_i < 4; k_i++) {
6             compute(spad_addr + k_i * 16, ...);
7
8 // Optimized
9 for (int k = 0; k < 8; k++) {
10     spad_addr = base_spad_addr;
11     dma_mvin(A[0][k*64], spad_addr);
12     for (int i = 0; i < 32; i++) {
13         dma_mvin(A[(i+1)*16][k*64], spad_addr + 64);
14         for (int k_i = 0; k_i < 4; k_i++) {
15             compute(spad_addr + k_i * 16, ...);
16         }
17     }
18     spad_addr += 64;

```

Figure 4: Example of software pipelining in tensor accelerators. The A matrix tile is spread throughout accelerator memory rather than repeatedly loaded to the same location, allowing data loading to run ahead and overlap with computation.

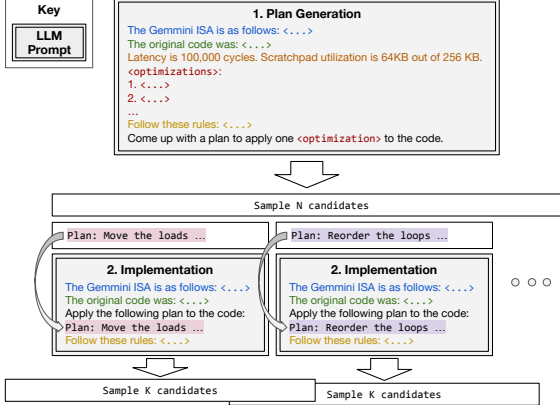


Figure 5: Autocomp’s two-phase optimization (Sec. 3.2) and carried out at each iteration of beam search.

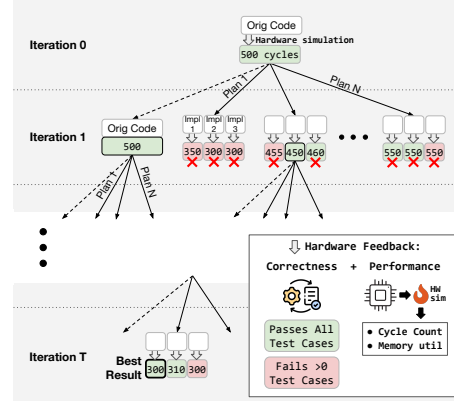


Figure 6: Autocomp’s beam search, described in Sec. 3.3.

to fine-tune models [55], construct simplified program abstractions for faster optimization [62], or utilize compiler and runtime feedback to iteratively improve the generated code [49, 11, 57, 47].

Some prior work, for example Ouyang et al. [47] and Taneja et al. [57], targets system-level performance programming, specifically CUDA and SIMD intrinsics. However, we are not aware of any works that address LLM code optimization for specialized hardware (i.e., not CPUs or GPUs). Hong et al. [22] show that zero-shot code generation for such languages is highly unreliable. Nonetheless, Autocomp successfully optimizes accelerator code via a combination of novel techniques.

3 The Autocomp Approach

3.1 Rationale

One naive way to generate optimized tensor accelerator code is to directly ask an LLM to rewrite the unoptimized code into its optimized counterpart. However, this approach fails for two reasons:

1. Tensor accelerator DSLs are low-resource languages (i.e., insufficiently represented in the LLM’s training corpus), so the model produces neither semantically nor syntactically valid programs.
2. Without guidance, the model has little notion of what optimizations to apply, or in which order.

Prior work shows that decomposing tasks, including code generation tasks, into multiple steps can improve an LLM’s ability to solve them [63, 15, 60, 22, 35]. Therefore, as shown in Fig. 5, we split our workflow into two phases: optimization plan generation and code implementation. We connect the two phases with an iterative beam search. Maintaining the best B code candidates at each step helps us explore multiple optimization trajectories in parallel. We describe our two phases and search strategy in the next section. Detailed prompts can be found in Appendix B.

In following sections, a *plan* refers to a natural language description of a single step of optimization and how code is transformed in that step, whereas a *schedule* refers to a sequence of plans that brings code from unoptimized to fully optimized.

3.2 Two-Phase Optimization

Phase 1: Optimization selection and plan generation. We prompt an LLM to select *one* optimization from a predefined menu of optimization options and to describe the concrete transformations required to apply it. Fig. 5 illustrates the prompt structure, which consists of the following parts:

1. **Accelerator ISA.** A list of instructions in the accelerator’s ISA. We describe the semantics of each instruction in natural language, provide a specification for the accelerator’s internal memory addresses, and briefly describe the accelerator’s structure.
2. **Current Code.** In the initial iteration $t = 0$, the original unoptimized code. When $t > 0$, one of the B candidates in our beam that has been selected for functional correctness and performance.

3. **Feedback.** The latency of **Current Code** in cycles, as well as its scratchpad and accumulator utilization in kilobytes. This helps the model choose the next optimization to apply. For example, low scratchpad utilization can lead to the model suggesting a larger tile transformation. Utilization is a common feedback metric across hardware platforms that reflects how effectively we are using the accelerator’s hardware resources.
4. **Optimization Menu.** A list of high-level optimizations, for instance, *loop unrolling, reordering, fusion, tiling*, and *double buffering*. Note that only the names of the optimization are included; we rely on model to generate the implementation details for the selected optimization. The full list of optimizations is in Appendix B.
5. **Instruction.** A simple natural-language directive to “select exactly one optimization from the menu and output a corresponding transformation plan.”
6. **Rules.** A set of constraints regarding the eventual code to be generated (see Appendix B).
7. **Beam Search Iteration.** We provide the current iteration number of the beam search, as well as the total number of iterations. This helps guide optimization selection, as some optimizations are more relevant towards the beginning of search (e.g., loop splitting), whereas some are more relevant towards the end of search (e.g., loop unrolling).

At each planning iteration, we sample N independent plans, seeding the search with multiple diverse optimization trajectories that can be evaluated in parallel.

Phase 2: Optimized code generation. Once we generate the candidate plans, for each plan we prompt the LLM to apply the transformations in the plan to generate a new, semantically equivalent code. In Fig. 5, we show the structure of our code generation prompt, which contains four parts:

1. **Accelerator ISA.** Same as in plan generation.
2. **Current Code.** Same as in plan generation.
3. **Generated Plan.** The specific optimization plan generated for this code in Phase 1.
4. **In-Context Learning (ICL) Example.** In cases where the optimization plan contains the string “tiling”, we provide an example of code (from a different workload, and with variable names anonymized) before and after changing one tiling factor. Inserted as tiling is a key optimization that requires modifications across the program, making it challenging to implement.
5. **Instruction.** A simple natural-language instruction to “apply the above plan and output optimized accelerator code that is functionally equivalent to the current code.”
6. **Rules.** Same as in plan generation.

We sample K independent code candidates for each plan because generating low-resource accelerator code is challenging, and also because our task also requires applying nontrivial transformations to the code. Sampling multiple candidates helps improve the robustness of our search process.

3.3 Beam Search

We integrate our two-phase optimization inside an iterative *beam search* of width B . Beam search allows us to efficiently explore several optimization trajectories in parallel. Since our code mostly consists of loop nests instead of sequential code, we find that merging candidates as in prior work [36, 4, 38, 37, 16, 51] is not suitable to tensor accelerator code. As illustrated in Fig. 6, candidates from the code generation step enter the beam only if they satisfy the criteria *correctness* and *performance*:

1. **Correctness.** After each code generation step, every candidate is compiled and run against our functional test suite. Each input variable is initialized with random values and after running, the candidate’s output is compared to that of a reference implementation. We first filter candidates by compiling and testing 5 times via functional hardware simulation, and up to 20 times in cycle-accurate simulation, which functionally matches real hardware at a cycle-level granularity.
2. **Performance.** We measure the latency of functionally correct candidates via cycle-accurate simulation. A candidate is retained only if it improves upon the parent from which it was derived.

Of the functionally correct candidates, we keep the best (lowest latency) B to seed the next iteration of beam search. Beam width is a hyperparameter, and empirically we found width $B = 6$ the sweet spot balancing search quality and time trade-off. We run this loop for a fixed budget of iterations.

3.4 Increasing Plan and Code Diversity

We use the following two techniques to boost the diversity in plan (and in the case of LLM ensembling, code) generation and prevent the model from repeatedly selecting the same optimization:

- **Optimization Menu Dropout.** Inspired by methods for preventing neural networks from overfitting [56], we implement dropout in our optimization menu. Each time a plan candidate is generated, each menu option in the list of optimizations has a chance to be dropped.
- **LLM Ensembling.** Ensembling LLMs is known to improve diversity and quality of results [28]. To further increase the diversity of generated plans and code, in each case where multiple candidates are sampled, we divide these requests between different LLMs.

We ablate these techniques, along with other components of Autocomp, in Appendix A.

3.5 Schedule Reuse

Running Autocomp’s search starting with unoptimized code results in optimized code that outperforms all prior approaches, as we will discuss in Sec. 4. However, using this approach with every new software workload can be costly, as Autocomp involves multiple LLM invocations and hardware simulations. A natural question, then, is whether the schedules discovered for one workload can be used to accelerate the optimization of others. We draw inspiration from traditional optimized libraries like BLAS [3], where hand-tuned schedules are reused across GEMM shapes, and extend Autocomp with schedule reuse.

To do so, we first record the best known schedule for a particular tensor operation. Then, during planning for new GEMMs with the same aspect ratios or with two shared dimensions, rather than exploring the full menu, we prompt the LLMs to select specifically the menu options used in our recorded schedule, one at a time. As we are not exploring the full menu, we can use a smaller beam width and sample count, reducing both LLM calls and search time. After completing this lightweight search, we take the best-performing code so far and further refine it by invoking the full Autocomp search for a small number of iterations. This resembles the classic exploration-exploitation trade-off in optimization: by reusing a schedule we exploit a known high-quality schedule and avoid the initial exploration cost for a new workload.

4 Evaluating Autocomp Without Schedule Reuse

We evaluate the effectiveness of Autocomp on three distinct types of workloads ¹: 1) matrix multiplication (GEMM) derived from ResNet-50, 2) convolution derived from ResNet-50, and 3) robotics code used for model-predictive control. For all experiments, we ensemble OpenAI’s o3-mini and gpt-4o (via the OpenAI API Platform) for both phases, with temperature 1.0. Menu options are dropped out with 70% probability.

4.1 Hardware Platform

We use Gemmini [17] to generate two different accelerators for evaluation. Gemmini is an accelerator generator that can generate systolic array- and vector-style tensor accelerators with a wide range of data types and sizes. Gemmini is ideal for evaluating Autocomp as it: 1) generates accelerators that deliver performance comparable to commercial ones, 2) is open-source, enabling instantiation of different accelerator instances, user modifications to the software toolchain, and extraction of fine-grained performance feedback, and 3) supports fast and cycle-accurate hardware simulation via FireSim [31]. Like other accelerators, its low-resource nature eliminates data contamination and makes directly prompting LLMs challenging. We used AWS EC2 F1 instances and local AMD Alveo U250 FPGAs to run FireSim.

For the GEMM and convolution benchmarks in Secs. 4.3 and 4.4, we use Gemmini to generate a 16×16 systolic array on 8-bit integer data type (accumulating in 32-bit), 256 KB scratchpad, and 64 KB accumulator, the same platform used by Ikarashi et al. [26]. For the fine-grained linear algebra benchmarks in Sec. 4.5, we generate a 32-bit floating point accelerator with a 4×4 systolic array, and

¹Benchmarks uploaded to <https://drive.google.com/drive/folders/1zK34x0tnzbQhcPjABxW-5uFbAKfoLGp6>

Approach	Performance	GEMM/conv size-agnostic	Supports workloads other than GEMM/conv	No power/area cost
Generic library (e.g. Gemmini SW Lib, Exo Unopt)	Low	✓	✗	✓
Hand tuning (e.g. Exo Opt)	Medium/High	✗	✓	✓
Hardware FSM	High	✓	✗	✗
Autocomp	High	✓	✓	✓

Table 1: Qualitative comparison of Autocomp to baseline approaches.

the same scratchpad and accumulator sizes, as used by Dong et al. [14]. This information is provided in the **Instruction** portion of our planning prompt.

4.2 Baselines

For the first two workload types, we compare Autocomp with four baselines, characterized in Table 1:

1. **Gemmini’s Software Library.** Gemmini ships with a software library that uses heuristics to tile and run GEMMs and convolutions on generated accelerators. As loop ordering is fixed and loop bounds, addresses, and indices must be computed at runtime, this implementation incurs significant software overhead and cannot fully utilize hardware resources.
2. **Exo Unoptimized.** Exo [26] is a DSL for tensor computation and scheduling. It comes with a basic compiler that emits functional GEMM or convolution code that can be executed on accelerators generated by Gemmini. However, without benchmark-specific optimization, performance is highly suboptimal, as hardware resources such as local memories tend to be underutilized.
3. **Exo Optimized.** In Ikarashi et al. [26], Exo’s and Gemmini’s developers spent significant effort manually writing and hand-tuning benchmark- and accelerator-specific schedules for each of the GEMM and convolution sizes in Figs. 7 and 8. This is the previous best known software implementation for these benchmarks.
4. **Hardware FSM.** Gemmini can generate accelerators with specialized hardware units for two coarse-grained operations: GEMM and convolution. These hardware units, implemented as finite state machines (FSMs), encode control sequences for each of these operations in hardware. If tuned correctly, the FSMs can exceed the theoretical maximum performance of any software-based implementation, as hardware is inherently parallel. However, this is accomplished at the cost of scheduling flexibility, as well as increased area, power, and hardware complexity. We use the hardware FSM as a reference for the highest achievable performance, but do not expect to exceed its performance for these GEMM/convolution benchmarks as its compute utilization exceeds 90% for all but one benchmark (82% on 12544x256x64). Despite this, Autocomp-generated code approach hardware FSM performance for GEMM/convolution, and as seen in Sec. 4.5, even exceeds hardware FSM performance in end-to-end application performance thanks to Autocomp’s greater scheduling flexibility.

For GEMM and convolution, we use Exo Unoptimized, which contains statically pre-computed loops, addresses, and indices, as Autocomp’s starting point. This simplifies code generation and allows us to directly compare the effectiveness of Autocomp to hand-optimization (i.e., Exo Optimized code).

The third workload type, robotics control code, is a multi-kernel application containing sequences of element-wise operations and matrix-vector multiplications. As this is not directly supported by Exo, we compare to an unoptimized software implementation ported to accelerator code by Dong et al. [14], and an extensively hand-optimized hardware FSM-based implementation written by an expert.

4.3 Matrix multiplication (GEMM)

We run Autocomp on a set of GEMM benchmarks selected by Ikarashi et al. [26] from ResNet-50 [19] for diversity in size and shape. We run search with beam size $B = 6$, $N = 6$ plans per element in the beam, $K = 2$ code candidates per plan, and $T = 15$ iterations. This takes around 5 hours to run.

Fig. 7 shows that Autocomp significantly outperforms even extensively hand-optimized code (Exo Opt) by a geomean of $1.4\times$, Exo Unoptimized code (the starting point of Autocomp’s search) by $2.9\times$, and Gemmini’s software library by $5.6\times$. Autocomp is consistent: its generated code always achieves at least 85% of the hardware FSM’s utilization (and 91% on average).

Autocomp especially outperforms prior implementations thanks to extensive exploration of software pipelining and double-buffering, which allows better overlapping of data movement and computation,

for example by double-buffering both the scratchpad and accumulator. In many cases, Autocomp’s exploration also leads to different tiling and loop ordering choices than hand-optimized code, reducing data movement. We qualitatively analyze Autocomp-generated GEMM code in detail in Appendix C.

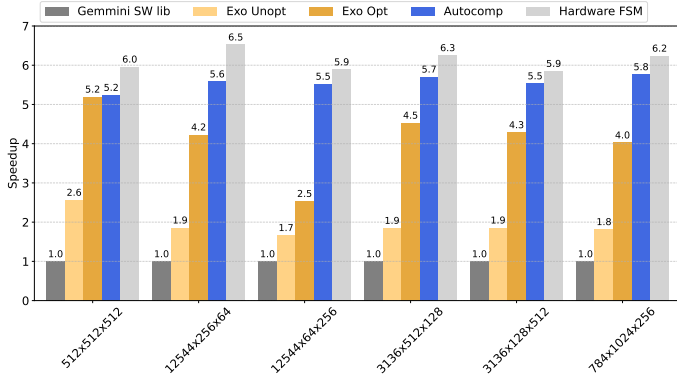


Figure 7: Speedup for **GEMM** benchmarks.

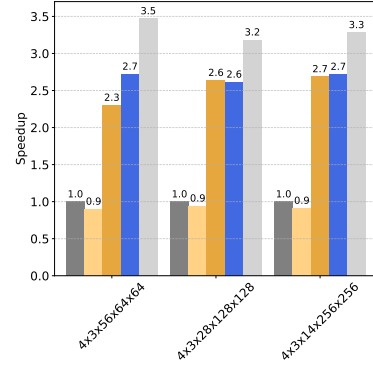


Figure 8: Speedup for **convolution** benchmarks.

4.4 Convolution

We also optimize convolution benchmarks from ResNet-50 via the same process. Compared to the GEMM benchmarks, this code contains more loops and is more complex. In this case, we run beam search with beam size $B = 6$, $N = 12$ plans, and $K = 4$ code candidates, for $T = 10$ iterations, which takes about 7 hours.

Compared to GEMM, convolution provides less room for improvement over both the Gemmini software library and Ikarashi et al. [26]’s implementation, as even the hardware FSM only achieves a $3.3 \times$ geomean speedup over the software library, compared to $6.1 \times$ for GEMM. This is because on average the Gemmini software library achieves 28% of the theoretical maximum compute utilization, compared to 16% for GEMM. As discussed by Genc et al. [17], at the tensor sizes in ResNet-50, convolutions have greater arithmetic intensity than GEMMs, making them less memory-bound and causing the Gemmini software library’s suboptimal data orchestration to be less impactful.

Nonetheless, as shown in Fig. 8, Autocomp still exceeds the previous best known hand-optimized software ISA-based implementation (Exo Opt) by up to $1.2 \times$ and by a geomean of $1.1 \times$, via similar strategies as for GEMM. It also outperforms Exo Unoptimized code by $2.9 \times$, and Gemmini’s software library by $2.6 \times$, and in all cases achieves at least 78% of the hardware FSM’s utilization.

4.5 Fine-Grained Linear Algebra

Finally, we optimize fine-grained linear algebra benchmarks from the TinyMPC model-predictive control library [40], specifically the forward and backward passes of the primal update step. These benchmarks contain sequences of floating-point matrix-vector multiplications, interleaved with element-wise addition and subtraction. The inclusion of CPU-accelerator dependencies, low reuse, and a high ratio of data movement to computation leads to low accelerator utilization and makes this code challenging to optimize.

We compare Autocomp-generated code against Dong et al. [14]’s unoptimized software-based implementation on a 4×4 FP32 accelerator. For this work, we additionally had an expert hand-tune a hardware FSM-based implementation. The unoptimized software-based implementation is used as the starting point for search, and we use the same search parameters as for convolution, except with $T = 15$ iterations, which takes about 12 hours. However, some of the optimization menu options are different from those used for GEMM/convolution (see Appendix B). As shown in Fig. 9, Autocomp outperforms even the expert-optimized hardware FSM implementation on the forward pass (by $1.6 \times$), and across benchmarks speeds up unoptimized code by a geomean of $2.7 \times$.

To outperform the hardware FSM implementation, Autocomp harnesses the flexibility of software-based implementation. It optimizes the code by hoisting data loads shared between kernels (reducing data movement beyond what is possible for the hardware FSM implementation), as well as utilizing

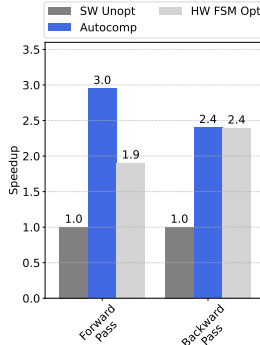


Figure 9: Speedup for **fine-grained linear algebra** benchmarks.

Category	Base Benchmark	Reuse Targets
Square	$1024 \times 1024 \times 1024$	$512 \times 512 \times 512, 256 \times 256 \times 256$
Column-dominant	$12544 \times 256 \times 64$	$6272 \times 256 \times 64, 12544 \times 128 \times 64$
Row-dominant	$128 \times 1024 \times 1024$	$64 \times 1024 \times 1024, 32 \times 1024 \times 1024$

Table 2: GEMM benchmarks for schedule reuse experiments.

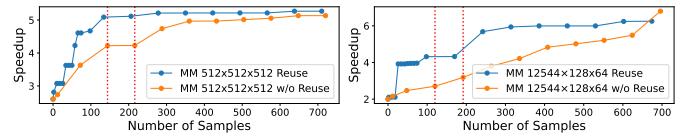


Figure 10: With the same sample budget, Autocomp with reuse (blue line) consistently delivers improved performance over Autocomp without reuse (orange line).

fine-grained software pipelining and eliminating blocking operations where possible. This experiment highlights Autocomp’s adaptability: we optimize a new benchmark, running on an accelerator with a new size and data type, with highly different performance characteristics from previous experiments, by updating the **Accelerator ISA** and changing a few lines in the **Optimization Menu** and **Instruction** sections of the prompt.

5 Improving Sample Efficiency With Schedule Reuse

In this experiment, we illustrate that optimization schedules generated by Autocomp for one tensor operation can be effectively reused to accelerate the optimization of similar tensor operations (as described in Sec. 3.5). For this experiment, we generate additional benchmarks structurally similar (either same aspect ratio or two shared dimensions) to those in Sec. 4.3. For each new benchmark, in the plan reuse phase, we search with beam size $B = 2$, $N = 2$ plan candidates, and $K = 2$ code candidates. Once the reuse sequence is exhausted, we switch to a full Autocomp search with beam size $B = 6$, $N = 6$ plan candidates, and $K = 2$ code candidates.

We consider GEMMs from the following categories: 1) square, 2) column-dominant and, 3) row-dominant, with dimensions specified in Table 2. The “base” benchmark is optimized using full search, i.e., without any schedule reuse, and its Autocomp generated schedule is then reused to optimize the other two benchmarks in its category.

We include the full optimization traces for Autocomp with and without reuse for two example benchmarks: $512 \times 512 \times 512$ (square) and $12544 \times 128 \times 64$ (column-dominant). As shown in Fig. 10, with reuse, Autocomp consistently achieves better speedups with the same number of samples.

For the remaining benchmarks, we perform an iso-samples comparison: we fix the total number of LLM calls and compare reuse to full search. In Fig. 10, the red vertical lines compare the iso-sample performance for our two examples. Across all reuse targets in Table 2, with a budget of 100 samples ($\approx 10\%$ of the calls used by full search), Autocomp achieves geomean speedups over Gemmini’s software library of $4.6 \times$ with reuse, compared to $3.7 \times$ without reuse. With a 200 call budget, we observe $5.0 \times$ speedup with reuse, compared to $4.2 \times$ without reuse. This demonstrates Autocomp schedules are generalizable and can help reduce the search cost when optimizing similar benchmarks.

6 Conclusion

In this paper, we demonstrate how to construct an LLM-based flow to automatically optimize low-resource accelerator code at superhuman levels. Autocomp outperforms the previous best known software implementation by generating code that is significantly faster on real-world benchmarks. By reducing the amount of manual effort needed to build compilers, we show the effectiveness of Autocomp’s approach and its potential to serve as a key component in the accelerator design process.

While Autocomp already delivers impressive performance across all benchmarks, in future work there is scope for broader plan reuse for greater sample efficiency. Currently, we only reuse individual

schedules; we can go further by extracting common patterns across schedules and summarizing them as “meta-schedules” which explain *how* to schedule and can be applied more broadly.

References

- [1] M. Acharya, Y. Zhang, K. Leach, and Y. Huang. Optimizing code runtime performance through context-aware retrieval-augmented generation, 2025. URL <https://arxiv.org/abs/2501.16692>.
- [2] S. Bhatia, J. Qiu, N. Hasabnis, S. A. Seshia, and A. Cheung. Verified code transpilation with llms. In A. Globerson, L. Mackey, D. Belgrave, A. Fan, U. Paquet, J. Tomczak, and C. Zhang, editors, *Advances in Neural Information Processing Systems*, volume 37, pages 41394–41424. Curran Associates, Inc., 2024. URL https://proceedings.neurips.cc/paper_files/paper/2024/file/48bb60a0c0aebb4142bf314bd1a5c6a0-Paper-Conference.pdf.
- [3] L. S. Blackford, A. Petitet, R. Pozo, K. Remington, R. C. Whaley, J. Demmel, J. Dongarra, I. Duff, S. Hammarling, G. Henry, et al. An updated set of basic linear algebra subprograms (blas). *ACM Transactions on Mathematical Software*, 28(2):135–151, 2002.
- [4] A. Chen, D. M. Dohan, and D. R. So. Evoprompting: Language models for code-level neural architecture search, 2023. URL <https://arxiv.org/abs/2302.14838>.
- [5] M. Chen, J. Tworek, H. Jun, Q. Yuan, H. P. d. O. Pinto, J. Kaplan, H. Edwards, Y. Burda, N. Joseph, G. Brockman, et al. Evaluating large language models trained on code. *arXiv preprint arXiv:2107.03374*, 2021.
- [6] T. Chen, Z. Du, N. Sun, J. Wang, C. Wu, Y. Chen, and O. Temam. DianNao: A Small-footprint High-throughput Accelerator for Ubiquitous Machine-learning. In *Proceedings of the International Conference on Architectural Support for Programming Languages and Operation Systems (ASPLOS)*, March 2014.
- [7] T. Chen, T. Moreau, Z. Jiang, L. Zheng, E. Yan, H. Shen, M. Cowan, L. Wang, Y. Hu, L. Ceze, C. Guestrin, and A. Krishnamurthy. TVM: An Automated End-to-end Optimizing Compiler for Deep Learning. In *USENIX Symposium on Operating Systems Design and Implementation (OSDI)*, 2018.
- [8] Y.-H. Chen, J. Emer, and V. Sze. Eyeriss: A Spatial Architecture for Energy-efficient Dataflow for Convolutional Neural Networks. In *Proceedings of the International Symposium on Computer Architecture (ISCA)*, 2016.
- [9] C. Cummins, B. Wasti, J. Guo, B. Cui, J. Ansel, S. Gomez, S. Jain, J. Liu, O. Teytaud, B. Steiner, Y. Tian, and H. Leather. Compilergym: robust, performant compiler optimization environments for ai research. In *Proceedings of the 20th IEEE/ACM International Symposium on Code Generation and Optimization*, CGO ’22, page 92–105. IEEE Press, 2022. ISBN 9781665405843. doi: 10.1109/CGO53902.2022.9741258. URL <https://doi.org/10.1109/CGO53902.2022.9741258>.
- [10] C. Cummins, V. Seeker, D. Grubisic, M. Elhoushi, Y. Liang, B. Roziere, J. Gehring, F. Gloeckle, K. Hazelwood, G. Synnaeve, et al. Large language models for compiler optimization. *arXiv preprint arXiv:2309.07062*, 2023.
- [11] S. Damani, S. K. S. Hari, M. Stephenson, and C. Kozyrakis. Warpdrive: An agentic workflow for ninja gpu transformations. In *Machine Learning for Systems Workshop at NeurIPS 2024*, 2024.
- [12] DeepSeek-AI, D. Guo, D. Yang, H. Zhang, J. Song, R. Zhang, R. Xu, Q. Zhu, S. Ma, P. Wang, X. Bi, X. Zhang, X. Yu, Y. Wu, Z. F. Wu, Z. Gou, Z. Shao, Z. Li, Z. Gao, A. Liu, B. Xue, B. Wang, B. Wu, B. Feng, C. Lu, C. Zhao, C. Deng, C. Zhang, C. Ruan, D. Dai, D. Chen, D. Ji, E. Li, F. Lin, F. Dai, F. Luo, G. Hao, G. Chen, G. Li, H. Zhang, H. Bao, H. Xu, H. Wang, H. Ding, H. Xin, H. Gao, H. Qu, H. Li, J. Guo, J. Li, J. Wang, J. Chen, J. Yuan, J. Qiu, J. Li, J. L. Cai, J. Ni, J. Liang, J. Chen, K. Dong, K. Hu, K. Gao, K. Guan, K. Huang, K. Yu, L. Wang, L. Zhang, L. Zhao, L. Wang, L. Zhang, L. Xu, L. Xia, M. Zhang, M. Tang, M. Li,

M. Wang, M. Li, N. Tian, P. Huang, P. Zhang, Q. Wang, Q. Chen, Q. Du, R. Ge, R. Zhang, R. Pan, R. Wang, R. J. Chen, R. L. Jin, R. Chen, S. Lu, S. Zhou, S. Chen, S. Ye, S. Wang, S. Yu, S. Zhou, S. Pan, S. S. Li, S. Zhou, S. Wu, S. Ye, T. Yun, T. Pei, T. Sun, T. Wang, W. Zeng, W. Zhao, W. Liu, W. Liang, W. Gao, W. Yu, W. Zhang, W. L. Xiao, W. An, X. Liu, X. Wang, X. Chen, X. Nie, X. Cheng, X. Liu, X. Xie, X. Liu, X. Yang, X. Li, X. Su, X. Lin, X. Q. Li, X. Jin, X. Shen, X. Chen, X. Sun, X. Wang, X. Song, X. Zhou, X. Wang, X. Shan, Y. K. Li, Y. Q. Wang, Y. X. Wei, Y. Zhang, Y. Xu, Y. Li, Y. Zhao, Y. Sun, Y. Wang, Y. Yu, Y. Zhang, Y. Shi, Y. Xiong, Y. He, Y. Piao, Y. Wang, Y. Tan, Y. Ma, Y. Liu, Y. Guo, Y. Ou, Y. Wang, Y. Gong, Y. Zou, Y. He, Y. Xiong, Y. Luo, Y. You, Y. Liu, Y. Zhou, Y. X. Zhu, Y. Xu, Y. Huang, Y. Li, Y. Zheng, Y. Zhu, Y. Ma, Y. Tang, Y. Zha, Y. Yan, Z. Z. Ren, Z. Ren, Z. Sha, Z. Fu, Z. Xu, Z. Xie, Z. Zhang, Z. Hao, Z. Ma, Z. Yan, Z. Wu, Z. Gu, Z. Zhu, Z. Liu, Z. Li, Z. Xie, Z. Song, Z. Pan, Z. Huang, Z. Xu, Z. Zhang, and Z. Zhang. Deepseek-r1: Incentivizing reasoning capability in llms via reinforcement learning, 2025. URL <https://arxiv.org/abs/2501.12948>.

[13] A. Developer. The scalable matrix extension (sme), for armv9-a, 2024. URL <https://developer.arm.com/documentation/ddi0616/latest/>.

[14] K. S. Dong, D. Nikiforov, W. Soedarmadji, M. Nguyen, C. Fletcher, and Y. S. Shao. Design space exploration of embedded soc architectures for real-time optimal control, 2024. URL <https://github.com/ucb-bar/Accelerated-TinyMPC/blob/main/Design-Space-Exploration-of-Embedded-SoC-Architectures-for-Real-Time-Optimal-Control.pdf>.

[15] L. Gao, A. Madaan, S. Zhou, U. Alon, P. Liu, Y. Yang, J. Callan, and G. Neubig. Pal: program-aided language models. In *Proceedings of the 40th International Conference on Machine Learning*, ICML’23. JMLR.org, 2023.

[16] S. Gao, C. Gao, W. Gu, and M. Lyu. Search-Based LLMs for Code Optimization . In *2025 IEEE/ACM 47th International Conference on Software Engineering (ICSE)*, pages 254–266, Los Alamitos, CA, USA, May 2025. IEEE Computer Society. doi: 10.1109/ICSE55347.2025.00021. URL <https://doi.ieee.org/10.1109/ICSE55347.2025.00021>.

[17] H. Genc, S. Kim, A. Amid, A. Haj-Ali, V. Iyer, P. Prakash, J. Zhao, D. Grubb, H. Liew, H. Mao, A. Ou, C. Schmidt, S. Steffl, J. Wright, I. Stoica, J. Ragan-Kelley, K. Asanovic, B. Nikolic, and Y. S. Shao. Gemmini: Enabling systematic deep-learning architecture evaluation via full-stack integration. In *2021 58th ACM/IEEE Design Automation Conference (DAC)*, 2021.

[18] I. J. Goodfellow, J. Pouget-Abadie, M. Mirza, B. Xu, D. Warde-Farley, S. Ozair, A. Courville, and Y. Bengio. Generative adversarial networks, 2014.

[19] K. He, X. Zhang, S. Ren, and J. Sun. Deep Residual Learning for Image Recognition. In *Proceedings of the Conference on Computer Vision and Pattern Recognition (CVPR)*, 2016.

[20] K. Hegde, P.-A. Tsai, S. Huang, V. Chandra, A. Parashar, and C. W. Fletcher. Mind mappings: enabling efficient algorithm-accelerator mapping space search. In *Proceedings of the 26th ACM International Conference on Architectural Support for Programming Languages and Operating Systems*, ASPLOS ’21, page 943–958, New York, NY, USA, 2021. Association for Computing Machinery. ISBN 9781450383172. doi: 10.1145/3445814.3446762. URL <https://doi.org/10.1145/3445814.3446762>.

[21] C. Hong, Q. Huang, G. Dinh, M. Subedar, and Y. S. Shao. Dosa: Differentiable model-based one-loop search for dnn accelerators. In *IEEE/ACM International Symposium on Microarchitecture (MICRO)*, 2023.

[22] C. Hong, S. Bhatia, A. Haan, S. K. Dong, D. Nikiforov, A. Cheung, and Y. S. Shao. Llm-aided compilation for tensor accelerators. In *2024 IEEE LLM Aided Design Workshop (LAD)*, pages 1–14, 2024. doi: 10.1109/LAD62341.2024.10691748.

[23] J. Hruska. As chip design costs skyrocket, 3nm process node is in jeopardy, 2018. URL <https://www.extremetech.com/computing/272096-3nm-process-node>.

[24] Q. Huang, M. Kang, G. Dinh, T. Norell, A. Kalaiah, J. Demmel, J. Wawrzynek, and Y. S. Shao. CoSA: Scheduling by Constrained Optimization for Spatial Accelerators. In *Proceedings of the International Symposium on Computer Architecture (ISCA)*, 2021.

[25] Q. Huang, C. Hong, J. Wawrynek, M. Subedar, and Y. S. Shao. Learning a continuous and reconstructible latent space for hardware accelerator design. In *Proceedings of the International Symposium on Performance Analysis of Systems and Software (ISPASS)*, 2022.

[26] Y. Ikarashi, G. L. Bernstein, A. Reinking, H. Genc, and J. Ragan-Kelley. Exocompilation for productive programming of hardware accelerators. In *Proceedings of the 43rd ACM SIGPLAN International Conference on Programming Language Design and Implementation*, PLDI 2022, page 703–718, New York, NY, USA, 2022. Association for Computing Machinery. ISBN 9781450392655. doi: 10.1145/3519939.3523446. URL <https://doi.org/10.1145/3519939.3523446>.

[27] Intel. Intel® advanced matrix extensions overview. URL <https://www.intel.com/content/www/us/en/products/docs/accelerator-engines/advanced-matrix-extensions/overview.html>.

[28] D. Jiang, X. Ren, and B. Y. Lin. LLM-blender: Ensembling large language models with pairwise ranking and generative fusion. In A. Rogers, J. Boyd-Graber, and N. Okazaki, editors, *Proceedings of the 61st Annual Meeting of the Association for Computational Linguistics (Volume 1: Long Papers)*, pages 14165–14178, Toronto, Canada, July 2023. Association for Computational Linguistics. doi: 10.18653/v1/2023.acl-long.792. URL <https://aclanthology.org/2023.acl-long.792>.

[29] N. P. Jouppi, C. Young, N. Patil, D. Patterson, G. Agrawal, R. Bajwa, S. Bates, S. Bhatia, N. Boden, A. Borchers, R. Boyle, P. luc Cantin, C. Chao, C. Clark, J. Coriell, M. Daley, M. Dau, J. Dean, B. Gelb, T. V. Ghaemmaghami, R. Gottipati, W. Gulland, R. Hagmann, C. R. Ho, D. Hogberg, J. Hu, R. Hundt, D. Hurt, J. Ibarz, A. Jaffey, A. Jaworski, A. Kaplan, H. Khaitan, D. Killebrew, A. Koch, N. Kumar, S. Lacy, J. Laudon, J. Law, D. Le, C. Leary, Z. Liu, K. Lucke, A. Lundin, G. MacKean, A. Maggiore, M. Mahony, K. Miller, R. Nagarajan, R. Narayanaswami, R. Ni, K. Nix, T. Norrie, M. Omernick, N. Penukonda, A. Phelps, J. Ross, M. Ross, A. Salek, E. Samadiani, C. Severn, G. Sizikov, M. Snelham, J. Souter, D. Steinberg, A. Swing, M. Tan, G. Thorson, B. Tian, H. Toma, E. Tuttle, V. Vasudevan, R. Walter, W. Wang, E. Wilcox, and D. H. Yoon. In-Datacenter Performance Analysis of a Tensor Processing Unit. In *Proceedings of the International Symposium on Computer Architecture (ISCA)*, 2017.

[30] S.-C. Kao, M. Pellauer, A. Parashar, and T. Krishna. Digamma: Domain-aware genetic algorithm for hw-mapping co-optimization for dnn accelerators. In *2022 Design, Automation & Test in Europe Conference & Exhibition (DATE)*, pages 232–237, 2022. doi: 10.23919/DATE54114.2022.9774568.

[31] S. Karandikar, H. Mao, D. Kim, D. Biancolin, A. Amid, D. Lee, N. Pemberton, E. Amaro, C. Schmidt, A. Chopra, Q. Huang, K. Kovacs, B. Nikolic, R. Katz, J. Bachrach, and K. Asanovic. Firesim: Fpga-accelerated cycle-exact scale-out system simulation in the public cloud. In *2018 ACM/IEEE 45th Annual International Symposium on Computer Architecture (ISCA)*, pages 29–42, 2018. doi: 10.1109/ISCA.2018.00014.

[32] A. Krizhevsky, I. Sutskever, and G. E. Hinton. Imagenet Classification with Deep Convolutional Neural Networks. 2012.

[33] H. Kwon, P. Chatarasi, V. Sarkar, T. Krishna, M. Pellauer, and A. Parashar. Maestro: A data-centric approach to understand reuse, performance, and hardware cost of dnn mappings. *IEEE Micro*, 40(3):20–29, 2020. doi: 10.1109/MM.2020.2985963.

[34] G. Lauterbach. The path to successful wafer-scale integration: the cerebras story. *IEEE Micro*, 41(6):52–57, 2021.

[35] C. Lee, A. Mahmoud, M. Kurek, S. Campanoni, D. Brooks, S. Chong, G.-Y. Wei, and A. M. Rush. Guess & sketch: Language model guided transpilation, 2024.

[36] J. Lehman, J. Gordon, S. Jain, K. Ndousse, C. Yeh, and K. O. Stanley. Evolution through large models, 2022. URL <https://arxiv.org/abs/2206.08896>.

[37] Y. J. Ma, W. Liang, G. Wang, D.-A. Huang, O. Bastani, D. Jayaraman, Y. Zhu, L. Fan, and A. Anandkumar. Eureka: Human-level reward design via coding large language models, 2024. URL <https://arxiv.org/abs/2310.12931>.

[38] M. U. Nasir, S. Earle, J. Togelius, S. James, and C. Cleghorn. Llmatic: Neural architecture search via large language models and quality diversity optimization. In *Proceedings of the Genetic and Evolutionary Computation Conference*, GECCO '24, page 1110–1118. ACM, July 2024. doi: 10.1145/3638529.3654017. URL <http://dx.doi.org/10.1145/3638529.3654017>.

[39] N. Nayak, T. O. Odemuyiwa, S. Ugare, C. Fletcher, M. Pellauer, and J. Emer. Teaal: A declarative framework for modeling sparse tensor accelerators. In *Proceedings of the 56th Annual IEEE/ACM International Symposium on Microarchitecture*, MICRO '23, page 1255–1270, New York, NY, USA, 2023. Association for Computing Machinery. ISBN 9798400703294. doi: 10.1145/3613424.3623791. URL <https://doi.org/10.1145/3613424.3623791>.

[40] K. Nguyen, S. Schoedel, A. Alavilli, B. Plancher, and Z. Manchester. Tinympc: Model-predictive control on resource-constrained microcontrollers. In *IEEE International Conference on Robotics and Automation (ICRA)*, 2024.

[41] E. Nijkamp, B. Pang, H. Hayashi, L. Tu, H. Wang, Y. Zhou, S. Savarese, and C. Xiong. Codegen: An open large language model for code with multi-turn program synthesis. *arXiv preprint arXiv:2203.13474*, 2022.

[42] NVIDIA. Nvdla, 2018. URL <https://nvdla.org/>.

[43] NVIDIA. About cuda, 2024. URL <https://developer.nvidia.com/about-cuda>.

[44] OpenAI. Introducing chatgpt, 2022. URL <https://openai.com/index/chatgpt/>.

[45] OpenXLA. Xla developer guide, 2024. URL <https://openxla.org/xla>.

[46] A. Orhon, A. Wadhwa, Y. Kim, F. Rossi, and V. Jagadeesh. Deploying transformers on the apple neural engine, Jun 2022. URL <https://machinelearning.apple.com/research/neural-engine-transformers>.

[47] A. Ouyang, S. Guo, S. Arora, A. L. Zhang, W. Hu, C. Ré, and A. Mirhoseini. Kernelbench: Can llms write efficient gpu kernels?, 2025. URL <https://arxiv.org/abs/2502.10517>.

[48] A. Parashar, P. Raina, Y. S. Shao, Y.-H. Chen, V. A. Ying, A. Mukkara, R. Venkatesan, B. Khailany, S. W. Keckler, and J. Emer. Timeloop: A systematic approach to dnn accelerator evaluation. In *Proceedings of the International Symposium on Performance Analysis of Systems and Software (ISPASS)*, 2019.

[49] Y. Peng, A. D. Gotmare, M. Lyu, C. Xiong, S. Savarese, and D. Sahoo. Perfcodegen: Improving performance of llm generated code with execution feedback, 2024. URL <https://arxiv.org/abs/2412.03578>.

[50] J. Ragan-Kelley, C. Barnes, A. Adams, S. Paris, F. Durand, and S. Amarasinghe. Halide: a language and compiler for optimizing parallelism, locality, and recomputation in image processing pipelines. In *Proceedings of the 34th ACM SIGPLAN Conference on Programming Language Design and Implementation*, PLDI '13, page 519–530, New York, NY, USA, 2013. Association for Computing Machinery. ISBN 9781450320146. doi: 10.1145/2491956.2462176. URL <https://doi.org/10.1145/2491956.2462176>.

[51] B. Romera-Paredes, M. Barekatain, A. Novikov, M. Balog, M. P. Kumar, E. Dupont, F. J. R. Ruiz, J. S. Ellenberg, P. Wang, O. Fawzi, P. Kohli, and A. Fawzi. Mathematical discoveries from program search with large language models. *Nat.*, 625(7995):468–475, January 2024. URL <http://dblp.uni-trier.de/db/journals/nature/nature625.html#RomeraParedesBNBKDRWFKF24>.

[52] C. Sakhija, Z. Shi, and C. Lin. Leveraging domain information for the efficient automated design of deep learning accelerators. In *International Symposium on High-Performance Computer Architectural (HPCA)*. IEEE, 2023.

[53] C. Sakhija, C. Hong, and C. Lin. Polaris: Multi-fidelity design space exploration of deep learning accelerators, 2024. URL <https://arxiv.org/abs/2412.15548>.

[54] A. Shilov. The golden age of custom silicon draws near: Part 3, 2023. URL <https://www.eetimes.com/the-golden-age-of-custom-silicon-draws-near-part-3/#:~:text=Meanwhile%20development%20of%20embedded%20software,not%20thousands%2C%20of%20titles%20flawlessly>.

[55] A. Shypula, A. Madaan, Y. Zeng, U. Alon, J. R. Gardner, Y. Yang, M. Hashemi, G. Neubig, P. Ranganathan, O. Bastani, et al. Learning performance-improving code edits. In *ICLR*, 2024.

[56] N. Srivastava, G. Hinton, A. Krizhevsky, I. Sutskever, and R. Salakhutdinov. Dropout: A simple way to prevent neural networks from overfitting. *Journal of Machine Learning Research*, 15(56):1929–1958, 2014. URL <http://jmlr.org/papers/v15/srivastava14a.html>.

[57] J. Taneja, A. Laird, C. Yan, M. Musuvathi, and S. K. Lahiri. Llm-vectorizer: Llm-based verified loop vectorizer. In *Proceedings of the 23rd ACM/IEEE International Symposium on Code Generation and Optimization*, CGO ’25, page 137–149, New York, NY, USA, 2025. Association for Computing Machinery. ISBN 9798400712753. doi: 10.1145/3696443.3708929. URL <https://doi.org/10.1145/3696443.3708929>.

[58] A. Tong, M. A. Cherney, and K. Hu. Exclusive: Openai set to finalize first custom chip design this year, Feb 2025. URL <https://www.reuters.com/technology/openai-set-finalize-first-custom-chip-design-this-year-2025-02-10/>.

[59] A. Vaswani, N. Shazeer, N. Parmar, J. Uszkoreit, L. Jones, A. N. Gomez, L. u. Kaiser, and I. Polosukhin. Attention is all you need. 2017.

[60] L. Wang, W. Xu, Y. Lan, Z. Hu, Y. Lan, R. K.-W. Lee, and E.-P. Lim. Plan-and-solve prompting: Improving zero-shot chain-of-thought reasoning by large language models. In A. Rogers, J. Boyd-Graber, and N. Okazaki, editors, *Proceedings of the 61st Annual Meeting of the Association for Computational Linguistics (Volume 1: Long Papers)*, pages 2609–2634, Toronto, Canada, July 2023. Association for Computational Linguistics. doi: 10.18653/v1/2023.acl-long.147. URL [https://aclanthology.org/2023.acl-long.147/](https://aclanthology.org/2023.acl-long.147).

[61] Y. Wang, W. Ye, P. Guo, Y. He, Z. Wang, Y. He, B. Tian, S. He, G. Sun, Z. Shen, S. Chen, A. Srivastava, Q. Zhang, G. Qu, and A. Li. Symrtlo: Enhancing rtl code optimization with llms and neuron-inspired symbolic reasoning, 2025. URL <https://arxiv.org/abs/2504.10369>.

[62] A. Wei, A. Nie, T. S. F. X. Teixeira, R. Yadav, W. Lee, K. Wang, and A. Aiken. Improving parallel program performance with llm optimizers via agent-system interface, 2025. URL <https://arxiv.org/abs/2410.15625>.

[63] J. Wei, X. Wang, D. Schuurmans, M. Bosma, B. Ichter, F. Xia, E. H. Chi, Q. V. Le, and D. Zhou. Chain-of-thought prompting elicits reasoning in large language models. In *Proceedings of the 36th International Conference on Neural Information Processing Systems*, NIPS ’22, Red Hook, NY, USA, 2022. Curran Associates Inc. ISBN 9781713871088.

[64] Q. Xiao, S. Zheng, B. Wu, P. Xu, X. Qian, and Y. Liang. Hasco: towards agile <u>ha</u>rdware and <u>s</u>oftware <u>co</u>-design for tensor computation. In *Proceedings of the 48th Annual International Symposium on Computer Architecture*, ISCA ’21, page 1055–1068. IEEE Press, 2021. ISBN 9781450390866. doi: 10.1109/ISCA52012.2021.00086. URL <https://doi.org/10.1109/ISCA52012.2021.00086>.

[65] D. Zhang, S. Huda, E. Songhori, K. Prabhu, Q. Le, A. Goldie, and A. Mirhoseini. A full-stack search technique for domain optimized deep learning accelerators. In *Proceedings of the 27th ACM International Conference on Architectural Support for Programming Languages and Operating Systems*, ASPLOS ’22, page 27–42, New York, NY, USA, 2022. Association for Computing Machinery. ISBN 9781450392051. doi: 10.1145/3503222.3507767. URL <https://doi.org/10.1145/3503222.3507767>.

[66] L. Zheng, R. Liu, J. Shao, T. Chen, J. Gonzalez, I. Stoica, and A. Haj-Ali. Tensem: A large-scale program performance dataset for learned tensor compilers. In J. Vanschoren and S. Yeung, editors, *Proceedings of the Neural Information Processing Systems Track on Datasets and Benchmarks*, volume 1, 2021. URL https://datasets-benchmarks-proceedings.neurips.cc/paper_files/paper/2021/file/a684ecee76fc522773286a895bc8436-Paper-round1.pdf.

A Ablation Studies

Experiment	12544x64x256 GEMM Speedup	4x3x14x256x256 Conv Speedup
Baseline (Exo Unopt)	1.67 \times	0.91 \times
No Accelerator ISA	3.11 \times	2.51 \times
No Optimization Menu	2.34 \times	0.97 \times
No Optimization Menu Dropout	4.72 \times	2.30 \times
No LLM Ensemble (o3-mini only)	4.67 \times	2.08 \times
No Hardware Perf Feedback	4.91 \times	2.61 \times
LLM Selection (DeepSeek-R1)	4.89 \times	2.25 \times
Autocomp	5.53\times	2.72\times

Table 3: Speedup relative to Gemmini’s software library for each of the studies in this section. We include two representative benchmarks, one GEMM and one convolution, from our initial evaluation.

In this section, we ablate various features of Autocomp to investigate their effect on optimization performance. We focus on two specific benchmarks from Sec. 4—our 12544x64x256 GEMM and our 4x3x14x256x256 convolution—to isolate the effects of these ablations while limiting the cost of running this extensive exploration.

A.1 Accelerator ISA

We find that for GEMM and convolution code, removing the ISA significantly deteriorates performance. Still, Autocomp is able to improve over the original code by a notable margin even without the ISA, given that all its other features are still enabled (see Table 3). This is because we inherently provide an example of accelerator ISA code at each step via the current code, so the model is able to infer some properties of the accelerator ISA. In addition, many of the nested loop optimizations for the GEMM and convolution workloads are well-understood transformations that operate on the C-syntax loops, addresses, and indices in the code, which resemble general-purpose programming, rather than using accelerator-specific constructs such as configuration instructions. However, full Autocomp performance is not matched as the proportion of functionally correct responses is lower, and instruction-level optimizations cannot easily be identified. For example, the first-compute handling optimization in Appendix C.1’s GEMM example and the negative-scaled bias loading in Appendix C.2’s fine-grained linear algebra example would not have been identified without knowledge of the ISA. Overall, we find that the accelerator ISA is an important part of Autocomp’s prompts.

A.2 Optimization Menu

We ablate the optimization menu by removing the menu in the planning prompt, and instead simply asking the model to select one optimization and generate a plan. From this experiment, we find that adding domain knowledge and optimization diversity via the optimization menu is essential to Autocomp. As shown in Table 3, optimization performance completely deteriorates without the optimization menu. Qualitatively, without the optimization menu, we find that the models tend to repeat similar optimizations, with significantly less diversity and relevance in the generated optimization plans.

A.3 Optimization Menu Dropout

“Dropout” for optimization menu options is a key contribution of this work that increases the diversity of generated optimization plans. Table 3 shows that menu dropout has a significant effect on performance. Qualitatively, we find that without dropout, models tend to be biased towards a limited set of menu options, a limitation which can be resolved via menu dropout.

A.4 Hardware Performance Feedback

As discussed in Sec. 3.2, during plan generation, we include the latency, scratchpad utilization, and accumulator utilization of the original code. Table 3 shows that this component is helpful,

but in some cases its effects may be limited. This is because the options listed in the optimization menu already capture some of the metrics measured in our performance feedback, for example the menu options which suggest using larger tile sizes. Hardware feedback such as scratchpad and accumulator utilization only serves to augment elaboration of these menu options by providing exact measurements.

A.5 LLM Ensembling

Splitting requests between LLMs in an ensemble also encourages diversity of generated plans and code. Qualitatively, we find that the responses, especially during the planning phase, generated by different LLMs differ substantially. Our experiments in Table 3 show that using individual models, such as o3-mini or DeepSeek-R1, on their own results in significantly lower performance.

A.6 LLM Selection

In Sec. 4, we use an ensemble of gpt-4o and o3-mini for our search. To demonstrate that Autocomp does not depend on a particular family of models, we run Autocomp with DeepSeek-R1 [12] on the same benchmarks used for other ablation experiments above. We use DeepSeek-R1 for both the planning and code generation phases and keep the search parameters identical to those used for matrix multiplication and convolution in Sec. 4. As shown in Table 3, Autocomp with DeepSeek-R1 is able to optimize both GEMM and convolution, achieving substantial speed-ups over the unoptimized code. These experiments do not use LLM ensembling. Similarly to the LLM ensembling ablation study above, gains are slightly smaller than when all techniques are applied. Nonetheless, this demonstrates that Autocomp is efficient and flexible across different LLMs.

B Prompts

```

#define config_ex(dataflow, act, A_stride, A_transpose, B_transpose)
// configure the state of the accelerator
// dataflow is WEIGHT_STATIONARY or OUTPUT_STATIONARY
// act is the activation function, options are NO_ACTIVATION, RELU, LAYERNORM, IGELU, SOFTMAX
// A_stride is the stride with which rows of A in the scratchpad are loaded into the systolic array, during
// computes. If this stride is 1, then we feed consecutive rows in the scratchpad, starting from the
// starting address of A, into the systolic array as the A matrix. If the stride is 2, then we feed every
// other row into the systolic array instead.
// A_transpose is a boolean value that represents whether the matrix A is transposed
// B_transpose is a boolean value that represents whether the matrix B is transposed

#define config_ld(dram_stride, scale_factor, spad_block_stride, id)
// configure mvin instructions
// dram_stride = stride in bytes, with which to load from DRAM
// scale_factor = factor to multiply loaded values
// spad_block_stride = when more than DIM columns are loaded, the distance in rows between each block of DIM
// columns
// id = id of mvin instruction; id = 0 for mvin, 1 for mvin2, 2 for mvin3

#define mvin(dram_addr, spad_acc_addr, cols, rows)
// mvin from DRAM to scratchpad or accumulator
// mvin, configured by config_ld(..., 0)
// rows must be less than or equal to DIM. If more than DIM rows, multiple mvin instructions are needed
// cols must be less than or equal to 4 * DIM.
// if dram_addr = 0, then zeroes are moved into scratchpad/accumulator, max size DIM x DIM

#define mvin2(dram_addr, spad_acc_addr, cols, rows)
// behavior identical to mvin, but configured by config_ld(..., 1)

#define mvin3(dram_addr, spad_acc_addr, cols, rows)
// behavior identical to mvin, but configured by config_ld(..., 2)

// A = input matrix, B = weight matrix, C = output matrix
// assume a weight-stationary dataflow
// preload, compute_preloaded, and compute_accumulated are used to compute DIM x DIM matrix multiplications.
// if no bias, C = A * B is computed; if there is a bias, C = A * B + bias is computed

#define preload(B_spad_addr, C_acc_addr, B_cols, B_rows, C_cols, C_rows)
// preload weights, B, onto DIM by DIM systolic array
// B must be preloaded before compute
// B must have been moved in to the scratchpad first
// B_cols must be less than or equal to DIM, B_rows must be less than or equal to DIM, C_cols must be less
// than or equal to DIM, C_rows must be less than or equal to DIM
// must run to change the output address to C_acc_addr
// if B_spad_addr unchanged from previous preload instruction, can set B_spad_addr = 0xffffffff; must be
// specified otherwise

#define compute_preloaded(A_spad_addr, bias_spad_addr, A_cols, A_rows, bias_cols, bias_rows)
// compute on DIM by DIM systolic array, with optional added bias (can be used for matrix addition)
// A must have been moved in to the scratchpad first
// first compute after preload to systolic array
// either overwrites or accumulates C depending on bit 30 of C_acc_addr
// A_cols must be less than or equal to DIM, A_rows must be less than or equal to DIM, bias_cols must be less
// than or equal to DIM, bias_rows must be less than or equal to DIM
// bias_spad_addr = 0xffffffff if no bias
// if there is a bias, bias_cols and bias_rows are probably equal to C_cols and C_rows from preload
// instruction

#define compute_accumulated(A_spad_addr, bias_spad_addr, A_cols, A_rows, bias_cols, bias_rows)
// compute on DIM by DIM systolic array
// A must have been moved in to the scratchpad first
// for weight stationary, use when B_spad_addr has not changed
// either overwrites or accumulates C depending on bit 30 of C_acc_addr
// A_cols must be less than or equal to DIM, A_rows must be less than or equal to DIM, bias_cols must be less
// than or equal to DIM, bias_rows must be less than or equal to DIM
// bias_spad_addr = 0xffffffff if no bias
// if there is a bias, bias_cols and bias_rows are probably equal to B_cols and B_rows from preload
// instruction

#define config_st(cols)
// configure mvout instruction
// cols = number of columns of matrix in DRAM

#define mvout(dram_addr, spad_acc_addr, cols, rows)
// mvout from scratchpad or accumulator to DRAM
// cols must be less than or equal to DIM
// rows must be less than or equal to DIM

#define fence() asm volatile("fence")
// fence

```

Figure 11: Accelerator ISA specification for Gemmini accelerators, referenced in Sec. 3.2.

```

,,,  

Gemmini's private memory is "row-addressed", where each row is DIM elements wide, where DIM is the number of  

PEs across the width of the systolic array. These elements will be of type inputType in the scratchpad,  

and of type accType in the accumulator.  

Every private Gemmini memory address is 32 bits long. The three most significant bits are reserved, and have  

special meanings:  

Bit 31 (the MSB) is 0 if we are addressing the scratchpad, and 1 if we are addressing the accumulator.  

Bit 30 is ignored if we are addressing the scratchpad, or if we are reading from the accumulator. If,  

instead, we are writing to the accumulator, then bit 30 is 0 if we want to overwrite the data at  

that address, and 1 if we want to accumulate on top of the data already at that address.  

Bit 29 is ignored if we are addressing the scratchpad, or if we are writing to the accumulator. If,  

instead, we are reading from the accumulator, then bit 29 is 0 if we want to read scaled-down  

inputType data from the accumulator, and 1 if we want to read accType data from the accumulator.  

If bit 29 is 1 for an accumulator read address, then we do not apply activation functions or scaling  

to the output of the accumulator.  

,,,  

,,,  

Gemmini is a decoupled access/execute architecture, which means that "memory-access" and "execute"  

instructions happen concurrently, in different regions of the hardware.  

It has an ExecuteController (for preload and compute instructions), LoadController (mvin), and StoreController  

(mvout).  

Gemmini includes an ROB which is meant to detect hazards between instructions in different controllers.  

Each controller also handles its own dependencies and hazards internally.  

,,  

""

```

Figure 12: Accelerator ISA specification from Sec. 3.2, continued.

```

<optimizations>:  

1. modify loop tiling  

2. loop reordering  

3. split loops  

4. fuse loops  

5. simplify arithmetic and propagate constants to simplify expressions  

6. reorder computations or blocks of computations  

7. loop unrolling  

8. double buffering  

9. move more data to the scratchpad in a more outer loop to increase data reuse  

10. spread data throughout the scratchpad rather than loading to the same location repeatedly  

11. load data to the scratchpad across outer loop iterations and use if statements to prevent  

    redundant loads on loops inner to those  

12. hoist redundant operations out of loops  

13. substitute operations with equivalent operations that are faster  

14. pipeline operations to better overlap computation and data movement  

15. minimize data movement  

16. minimize loop overhead  

17. other methods not listed here.

```

Figure 13: The list of optimizations menu options available (with some probability of dropout)
during the planning phase, as described in Sec. 3.2. This menu was used to optimize both matrix
multiplication and convolution code.

```

<optimizations>:  

1. remove unnecessary code  

2. simplify arithmetic and propagate constants to simplify expressions  

3. merge instructions  

4. merge high-level operations  

5. reorder operations or blocks of operations  

6. move cpu-based computation to the accelerator  

7. add or subtract a matrix using the bias  

8. hoist redundant operations out of loops  

9. substitute operations with equivalent operations that are faster  

10. pipeline operations to better overlap computation and data movement  

11. eliminate data dependencies and fence operations  

12. minimize data movement  

13. minimize loop overhead  

14. other methods not listed here

```

Figure 14: The optimization menu for TinyMPC code optimization.

```

Here is an example of increasing scratchpad tile size for the Y dimension of a 512x512 (X x Z) matrix A and
512x512 (Z x Y) matrix B multiplication. Original code:
uint32_t b_offset = 16 * 16 * 4 * 8 * sizeof(int8_t);
for (int_fast32_t y = 0; y < 8; y++) {
    uint32_t b_base_y = 64 * y;
    // Load B matrix slice
    for (int_fast32_t zo = 0; zo < 8; zo++) {
        uint32_t b_zo_offset = 4 * 16 * zo; // Number of columns per zo iteration
        for (int_fast32_t z = 0; z < 4; z++) {
            uint32_t b_index = ((zo * 4 + z) * ((16 * 4) * 16)) / 16; // Divide number of elements by 16
            // since scratchpad is row-indexed
            mvn3(&B[b_zo_offset + 16 * z][b_base_y], b_offset + b_index, 16 * 4, 16);
        }
    }
    for (int_fast32_t x = 0; x < 32; x++) {
        uint32_t res = 1 << 31;
        uint32_t a_base_x = 16 * x;
        // Load A matrix slice
        for (int_fast32_t zo = 0; zo < 8; zo++) {
            uint32_t a_index = (zo * (16 * 4) * 16) / 16;
            mvn2(&A[a_base_x][64 * zo], a_index, 16 * 4, 16);
        }
        // Computation
        for (int_fast32_t zo = 0; zo < 8; zo++) {
            uint32_t a_index = (zo * (16 * 4) * 16) / 16;
            for (int_fast32_t z = 0; z < 4; z++) {
                uint32_t preload_flag = (zo == 0 && z == 0) ? 0 : 0x40000000;
                for (int_fast32_t y_in_o = 0; y_in_o < 4; y_in_o++) {
                    uint32_t preload_index = ((zo * 4 + z) * ((16 * 4) * 16) + y_in_o * (16 * 16)) / 16;
                    // Find correct scratchpad index to load B from
                    preload(b_offset + preload_index, res + (y_in_o * (16 * 16)) / 16 | preload_flag, 16,
                           16, 16, 16);
                    compute_preloaded(a_index + (z * (16 * 16)) / 16, ~((uint32_t)0), 16, 16, 16, 16);
                }
            }
        }
        // Store C matrix slice
        for (int_fast32_t y_in_o = 0; y_in_o < 4; y_in_o++) {
            mvout(&C[a_base_x][b_base_y + 16 * y_in_o], res + (y_in_o * (16 * 16)) / 16, 16, 16); // Divide number of elements by 16 since accumulator is row-indexed
        }
    }
}

Retiled code
uint32_t b_offset = 16 * 16 * 4 * 8 * sizeof(int8_t);
for (int_fast32_t y = 0; y < 2; y++) { // Reduce number of y dimension outer loop iterations
    uint32_t b_base_y = 256 * y;
    // Load larger B matrix slice
    // Tiling reduces redundant loads of B matrix, reducing data movement and increasing data reuse
    for (int_fast32_t zo = 0; zo < 8; zo++) {
        uint32_t b_zo_offset = 4 * 16 * zo; // Number of columns per zo iteration
        for (int_fast32_t z = 0; z < 4; z++) {
            for (int_fast32_t y_in = 0; y_in < 4; y_in++) {
                uint32_t b_index = (((zo * 4 + z) * 4 + y_in) * ((16 * 4) * 16)) / 16; // Divide number of elements by 16 since scratchpad is row-indexed
                mvn3(&B[b_zo_offset + 16 * z][b_base_y + 64 * y_in], b_offset + b_index, 16 * 4, 16);
            }
        }
    }
    for (int_fast32_t x = 0; x < 32; x++) {
        uint32_t res = 1 << 31;
        uint32_t a_base_x = 16 * x;
        // Load A matrix slice
        // Tiling reduces redundant loads of A matrix, reducing data movement and increasing data reuse
        for (int_fast32_t zo = 0; zo < 8; zo++) {
            uint32_t a_index = (zo * (16 * 4) * 16) / 16;
            mvn2(&A[a_base_x][64 * zo], a_index, 16 * 4, 16);
        }
        // Computation
        for (int_fast32_t zo = 0; zo < 8; zo++) {
            uint32_t a_index = (zo * (16 * 4) * 16) / 16;
            for (int_fast32_t z = 0; z < 4; z++) {
                uint32_t preload_flag = (zo == 0 && z == 0) ? 0 : 0x40000000;
                for (int_fast32_t y_in_o = 0; y_in_o < 16; y_in_o++) { // Increase number of Y dimension inner loop iterations to increase tile size
                    uint32_t preload_index = (((zo * 4 + z) * 4) * ((16 * 4) * 16) + y_in_o * (16 * 16)) / 16; // Find correct scratchpad index to load B from
                    preload(b_offset + preload_index, res + (y_in_o * (16 * 16)) / 16 | preload_flag, 16,
                           16, 16, 16);
                    compute_preloaded(a_index + (z * (16 * 16)) / 16, ~((uint32_t)0), 16, 16, 16, 16);
                }
            }
        }
        // Store C matrix slice
        for (int_fast32_t y_in_o = 0; y_in_o < 16; y_in_o++) { // Move out a larger tile in the Y dimension
            mvout(&C[a_base_x][b_base_y + 16 * y_in_o], res + (y_in_o * 16 * 16) / 16, 16, 16); // Divide number of elements by 16 since accumulator is row-indexed
        }
    }
}

```

Figure 15: In-context learning example of tiling, provided during the code generation phase in Sec. 3.2. Inserted in the prompt only when the string "tiling" is detected in the plan generated in Phase 1.

Rules:

1. The rewritten program should be semantically equivalent to the original program
2. Limit the scope of the plan to the selected optimization
3. All code must be inside the test() function
4. Do not use C preprocessing directives (#ifdef, #define, etc.)
5. If modifying loops, modify other related loop bounds and adjust address and index calculations to ensure the code is still correct
6. If increasing loaded tile size, ensure that data is spread throughout the scratchpad across all relevant dimensions
7. If loading across new dimensions, add the loop indices of those dimensions to scratchpad address calculations
8. If increasing loaded tile size, update preload and compute instructions to match the new data layout
9. If increasing loaded tile size, update base scratchpad addresses to fit new tile size

Figure 16: The list of rules provided during both the planning and code implementation phases, as described in Sec. 3.2.

C Code Examples

In this section, we discuss in greater depth what optimizations Autocomp applies in our evaluations and how Autocomp is able to achieve significantly better performance than hand-optimized code.

C.1 12544x64x256 GEMM

Fig. 17 contains the unoptimized Exo-generated code, used as the starting point for search. Fig. 18 contains the code generated by Exo after hand-optimization by Ikarashi et al. [26]. Figs. 19 to 21 contain the result of Autocomp optimization on Exo Unoptimized code. While the code is substantially transformed from the original code, some aspects remain the same. For example, in this case the configuration instructions and loop ordering remain largely the same.

Of course, many optimizations have been applied to the code. We briefly summarize the optimization menu options selected and plans generated during the optimization process for this code. We also include the speedup after each respective optimization.

1. $1.67\times$: initial speedup of Exo Unoptimized code over Gemmini’s software library before any optimization.
2. $1.93\times$ after “hoist redundant operations out of loops”. This plan hoists constants like `tile_dim = 16` and loop-invariant expressions like `ko * 64` and `k * 16` out of inner loops. These precomputed values are reused inside Gemmini ops in each iterations, so we should reduce the number of times they must be calculated.
3. $1.95\times$ after “double buffering”. This plan defines two buffer regions for matrices A and B in the scratchpad. A `buffer_toggle` flag is introduced to alternate between these buffers each iteration. All `mvn`, `preload`, and `compute` instructions are updated to use the active buffer based on the toggle. Data loading for the next iteration is scheduled earlier to overlap with current computation. Address calculations are adjusted to include buffer offsets accordingly.
4. $2.15\times$ after “pipeline operations to better overlap computation and data movement”. Moves `mvn2` (A tile load) to immediately after `compute_preloaded` in the `ko` loop to overlap A prefetch with current compute. Moves `mvn3` (B tile load) earlier in the `k` loop, before the next compute, to overlap B prefetch with current compute.
5. $3.13\times$ after “load data to the scratchpad across outer loop iterations and use if statements to prevent redundant loads on loops inner to those”. Adds a one-time load of the entire B matrix into a new scratchpad region (specifically, `new_B_base = 8192`) before the main `i` loop. Replaces repeated `mvn3` calls in inner loops with offset calculations into this preloaded B region.
6. $3.54\times$ after “move more data to the scratchpad in a more outer loop to increase data reuse”. Before the reduction (`k`) loop, load the entire 16×256 A-tile into scratchpad using four `mvn2` calls to a new `A_tile_base` region. Remove the double-buffering (`a_toggle`) for A since the full tile is now resident. Replace nested `ko` and `k` loops with a single loop over 16 segments, computing each 16×16 A sub-tile address from `A_tile_base`. Adjust B tile preload and `compute_preloaded` calls accordingly, using a simpler tile index.
7. $4.87\times$ after “double buffering”. Restores double buffering by reserving two scratchpad regions: `A_tile_base0` and `A_tile_base1`, each holding one full 16×256 A-tile. In the outer `i` loop, alternate buffers using `i % 2` to select `current_buffer` and `next_buffer`. In each iteration (except last), while computing with `current_buffer`, issue `mvn2` to load the next A-tile into `next_buffer`. In the inner `compute` loops, use `current_buffer` for A-tile addresses. After `compute` and `mvout`, the next iteration uses the preloaded data.
8. $5.21\times$ after “double buffering”. Double-buffers accumulator by allocating two accumulator regions: `acc_base0` and `acc_base1`. In each `i` iteration, `compute` into `cur_acc_base` and `mvout` from `prev_acc_base` (except on first iteration), and swap `cur_acc_base` and `prev_acc_base` at the end of the loop.
9. $5.23\times$ after “loop unrolling”. Unrolls the innermost loop (`j_in_o`) by a factor of 4.
10. $5.53\times$ after “fuse loops”. “Fuses” loops by eliminating the loop over `j_in_o` where we `mvn 0s` to the accumulator. Instead, use the ability of `preload` to overwrite the values in the accumulator rather than accumulating, when beginning a new partial sum.

From this example, we observe that a diverse set of optimizations is selected, and that speedups are distributed throughout the optimization process rather than concentrated in just one or two steps, showing the importance of a well-designed iterative search process. From here, we summarize the differences between Autocomp-generated code and the previous best code (Exo Opt):

- **Tiling.** The Exo Opt code loads 128×256 tiles of A, whereas the Autocomp-generated code loads 32×256 tiles (divided into two 16×256 tiles) of A. While this means there is less reuse for the Autocomp-generated code, there is also less overhead needed for compute instructions to wait for each A tile to be loaded to the scratchpad. In combination with the rest of the optimizations applied by Autocomp, this leads to improved performance.
- **Double-buffering.** In the Autocomp-generated code, we see that both the scratchpad and accumulator are explicitly double-buffered. In the schedule, we can see that double buffering is applied 3 times. Initially (in step 3), both the A and B matrices (where matrix multiplication is represented as $A \times B = C$), are double buffered in the scratchpad. However, after steps 5 and 6, B and A (respectively) are no longer double-buffered as larger tiles are loaded before beginning computation. The accumulator is double-buffered in step 8, resulting in the code below. The Exo Opt code relies on the accelerator’s out-of-order execution to handle executing `mvin` and `mvout` instructions without dependencies, ahead of the order in which they are issued.
- **Software pipelining.** The Autocomp-generated code explicitly issues A `mvin` instructions before they are needed for computation, whereas as above the Exo Opt code relies on hardware to handle overlapping of data movement and compute. Also, the Autocomp-generated code explicitly issues all B `mvin` instructions at the beginning of the program, whereas the Exo Opt code interleaves these instructions with computation (but still loads the entire B matrix to the scratchpad, once overall). This does not have a significant impact on performance, but LLM-generated code is naturally biased towards such an implementation due to its simplicity.
- **First-compute handling.** The Autocomp-generated code utilizes the ability of compute instructions to overwrite the accumulator, whereas Exo Opt code explicitly issues `mvin` instructions to zero out the accumulator before beginning computation on a tile.
- **Arithmetic simplification.** Arithmetic on constants is fully simplified and handled inside shared variables wherever possible in the Autocomp-generated code, reducing the overhead of non-accelerator instructions.

Overall, we find that compared to the Exo Opt code, Autocomp-generated code applies more techniques to minimize the amount of CPU overhead during execution. The smaller tiles it uses, in combination with its more explicit application of double-buffering and software pipelining, results in highly tuned, fine-grained overlapping of data movement and computation and a very high level of performance.

C.1.1 Unoptimized Code Example

```

void test(int8_t A[12544][256], int8_t B[256][64], int8_t C[12544][64]) {
    config_st((64));
    config_ex(WEIGHT_STATIONARY, NO_ACTIVATION, 1, false, false);
    config_ld((64), 1.0f, 16, 2);
    config_ld((256), 1.0f, 16, 1);
    config_ld(0, 1.0f, 0, 0);

    for (int_fast32_t i = 0; i < 784; i++) {
        for (int_fast32_t j = 0; j < 1; j++) {
            uint32_t res = 1 << 31;
            for (int_fast32_t j_in_o = 0; j_in_o < 4; j_in_o++) {
                mvin( 0, res + ((j_in_o) * (256))/16, (16 + 0), (16 + 0) );
            }
            uint32_t a = 0;
            uint32_t b = 16 * 16 * 4 * 4 / 16;
            for (int_fast32_t ko = 0; ko < 4; ko++) {
                mvin2( &A[(16 * i)][64 * ko], a + ((ko) * (1024))/16, 16*(4 + 0), (16 + 0) );
                for (int_fast32_t k = 0; k < 4; k++) {
                    mvin3( &B[(64 * ko + 16 * k)][64 * j], b + ((ko) * (4096) + (k) * (1024))/16, 16*(4 + 0), (16 + 0) );
                }
                for (int_fast32_t k = 0; k < 4; k++) {
                    for (int_fast32_t j_in_o = 0; j_in_o < 4; j_in_o++) {
                        preload(b + ((ko) * (4096) + (k) * (1024) + (j_in_o) * (256))/16, res + ((j_in_o) * (256))/16 | 0
                            x40000000, (16 + 0), (16 + 0), (16 + 0), (16 + 0));
                        compute_preloaded(a + ((ko) * (1024) + (k) * (256))/16, ~((uint32_t)0), (16 + 0), (16 + 0), 16,
                            16);
                    }
                }
                for (int_fast32_t j_in_o = 0; j_in_o < 4; j_in_o++) {
                    mvout( &C[(16 * i)][16 * j_in_o + 64 * j], res + ((j_in_o) * (256))/16, (16 + 0), (16 + 0) );
                }
            }
        }
    }
    fence();
}

```

Figure 17: Example of Exo-generated unoptimized matrix multiplication code, from the experiments in Sec. 4.3. Achieves 28% utilization.

C.1.2 Exo Optimized Code Example

Figure 18: Example of hand-optimized matrix multiplication code from Ikarashi et al. [26], used as a baseline in Sec. 4.3. Achieves 43% utilization. Note that unrolled preload/compute_preloaded instructions have been truncated due to length.

C.1.3 Autocomp-Optimized Code Example

```

void test(int8_t A[12544][256], int8_t B[256][64], int8_t C[12544][64]) {
    //-----
    // Tile and matrix constants
    //-----

    const uint32_t tile_dim      = 16;    // tile dimension
    const uint32_t tile_offset = tile_dim; // each row in a tile is tile_dim elements

    // For double buffering, we use two accumulator base addresses separated by 4 tile rows.
    const uint32_t acc_base0 = 1U << 31;
    const uint32_t acc_base1 = (1U << 31) + (4 * tile_dim);

    const uint32_t new_B_base   = 8192;
    const uint32_t A_tile_base0 = 2048;
    const uint32_t A_tile_base1 = 6144;

    //-----
    // Gemmini configuration
    //-----

    config_st(64);
    config_ex(WEIGHT_STATIONARY, NO_ACTIVATION, 1, false, false);
    config_ld(64, 1.0f, tile_dim, 2);
    config_ld(256, 1.0f, tile_dim, 1);
    config_ld(0, 1.0f, 0, 0);

    //-----
    // Load the entire weight matrix B into the scratchpad once.
    //-----

    for (int br = 0; br < 256; br += tile_dim) {
        mvin3(&B[br][0],
              new_B_base + (br / tile_dim) * (tile_dim * 4),
              tile_dim * 4,
              tile_dim);
    }

    //-----
    // Begin double-buffered accumulator computation.
    //
    // cur_acc_base: where the current tile is computed.
    // prev_acc_base: holds the result of the previously computed tile.
    //-----

    uint32_t cur_acc_base = acc_base0;
    uint32_t prev_acc_base = 0; // Will be set after the first iteration.

    // Outer loop over tiles (784 tiles along A's first dimension)
    for (int i = 0; i < 784; i++) {

        // Determine which scratchpad region holds A for this tile.
        // Alternating between two buffers allows overlapping the load of the next tile.
        uint32_t current_A_buffer = (i % 2 == 0) ? A_tile_base0 : A_tile_base1;
        uint32_t next_A_buffer   = (i % 2 == 0) ? A_tile_base1 : A_tile_base0;

        //-----
        // For the first iteration load the A tile into scratchpad.
        // For subsequent iterations, write the previous tile from the accumulator.
        //-----
        if (i == 0) {
            for (int b = 0; b < 4; b++) {
                mvin2(&A[tile_dim * i][64 * b],
                      current_A_buffer + b * (tile_dim * 4),
                      tile_dim * 4,
                      tile_dim);
            }
        } else {
            for (int j_in_o = 0; j_in_o < 4; j_in_o++) {
                uint32_t j_off = j_in_o * tile_dim;
                mvout(&C[tile_dim * (i - 1)][tile_dim * j_in_o],
                      prev_acc_base + j_off,
                      tile_dim,
                      tile_dim);
            }
        }
    }
}

```

Figure 19: Example of an optimized version of the same GEMM from Fig. 17, generated using Autocomp. Achieves 93% compute utilization. Continued in Figs. 20 and 21.

```

//-----
// Instead of explicitly zeroing-out the accumulator tile via extended mvn,
// we fuse the accumulator zeroing into the compute stream.
//
// For each accumulator sub-tile (indexed by j_in_o), the very first compute
// call is issued in overwrite mode (i.e. the accumulator address is used as-is)
// and then all subsequent compute calls for that sub-tile are issued in accumulate mode.
//
// We use an array (first_compute) to track whether a given sub-tile has been updated.
//-----
int first_compute[4] = { 1, 1, 1, 1 };

//-----
// Compute the current tile.
// The complete computation is divided into 16 segments.
// Loop unrolling by a factor of 4 is applied to the segments loop.
//-----
for (int seg = 0; seg < 16; seg += 4) {
    for (int j_in_o = 0; j_in_o < 4; j_in_o++) {
        uint32_t j_off = j_in_o * tile_dim;
        uint32_t acc_addr; // will hold the computed accumulator address for preload

        //--- Unrolled segment "seg" -----
        {
            uint32_t block_id    = seg / 4;
            uint32_t sub_offset = (seg % 4) * tile_dim;
            uint32_t A_seg_addr = current_A_buffer + block_id * (tile_dim * 4) + sub_offset;
            // If this is the very first compute for this sub-tile, use overwrite mode
            if (first_compute[j_in_o]) {
                acc_addr = cur_acc_base + j_off;
                first_compute[j_in_o] = 0;
            } else {
                acc_addr = (cur_acc_base + j_off) | 0x40000000;
            }
            preload(new_B_base + seg * (tile_dim * 4) + j_off,
                   acc_addr,
                   tile_dim, tile_dim,
                   tile_dim, tile_dim);
            compute_preloaded(A_seg_addr,
                               ~(uint32_t)0,
                               tile_dim, tile_dim,
                               tile_dim, tile_dim);
        }

        //--- Unrolled segment "seg+1" -----
        {
            uint32_t block_id    = (seg + 1) / 4;
            uint32_t sub_offset = ((seg + 1) % 4) * tile_dim;
            uint32_t A_seg_addr = current_A_buffer + block_id * (tile_dim * 4) + sub_offset;
            preload(new_B_base + (seg + 1) * (tile_dim * 4) + j_off,
                   (cur_acc_base + j_off) | 0x40000000,
                   tile_dim, tile_dim,
                   tile_dim, tile_dim);
            compute_preloaded(A_seg_addr,
                               ~(uint32_t)0,
                               tile_dim, tile_dim,
                               tile_dim, tile_dim);
        }

        //--- Unrolled segment "seg+2" -----
        {
            uint32_t block_id    = (seg + 2) / 4;
            uint32_t sub_offset = ((seg + 2) % 4) * tile_dim;
            uint32_t A_seg_addr = current_A_buffer + block_id * (tile_dim * 4) + sub_offset;
            preload(new_B_base + (seg + 2) * (tile_dim * 4) + j_off,
                   (cur_acc_base + j_off) | 0x40000000,
                   tile_dim, tile_dim,
                   tile_dim, tile_dim);
            compute_preloaded(A_seg_addr,
                               ~(uint32_t)0,
                               tile_dim, tile_dim,
                               tile_dim, tile_dim);
        }
    }
}

```

Figure 20: Example from Fig. 19, continued.

```

----- Unrolled segment "seg+3" -----
{
    uint32_t block_id    = (seg + 3) / 4;
    uint32_t sub_offset = ((seg + 3) % 4) * tile_dim;
    uint32_t A_seg_addr = current_A_buffer + block_id * (tile_dim * 4) + sub_offset;
    preload(new_B_base + (seg + 3) * (tile_dim * 4) + j_off,
           (cur_acc_base + j_off) | 0x40000000,
           tile_dim, tile_dim,
           tile_dim, tile_dim);
    compute_preloaded(A_seg_addr,
                      ~(uint32_t)0,
                      tile_dim, tile_dim,
                      tile_dim, tile_dim);
}
} // end inner loop over j_in_o

-----
// For seg==0 (i.e. the first unrolled iteration), launch prefetching of the next A tile
.
// This overlaps memory-access with computation.
-----
if (seg == 0 && i < 783) {
    for (int b = 0; b < 4; b++) {
        mvin2(&A[tile_dim * (i + 1)][64 * b],
              next_A_buffer + b * (tile_dim * 4),
              tile_dim * 4,
              tile_dim);
    }
}
} // end segments loop

-----
// Swap accumulator buffers.
// The tile computed in this iteration (in cur_acc_base) becomes the previous tile,
// so it must be written back in the next iteration.
-----
prev_acc_base = cur_acc_base;
cur_acc_base = (cur_acc_base == acc_base0) ? acc_base1 : acc_base0;
} // end outer tile loop

-----
// Write back the final computed tile (tile index 783) from the accumulator.
-----
for (int j_in_o = 0; j_in_o < 4; j_in_o++) {
    uint32_t j_off = j_in_o * tile_dim;
    mvout(&C[tile_dim * (784 - 1)][tile_dim * j_in_o],
          prev_acc_base + j_off,
          tile_dim,
          tile_dim);
}
fence();
}

```

Figure 21: Example from Figs. 19 and 20, continued.

C.2 TinyMPC Primal Update Forward Pass (Fine-Grained Linear Algebra)

The forward pass of the TinyMPC primal update step computes the following operations:

$$\begin{aligned} u[i] &= -K_{inf} * x[i] - d[i] \\ x[i + 1] &= (A_{dyn} * x[i]) + (B_{dyn} * u[i]) \end{aligned}$$

Where A_{dyn} is a 12x12 matrix, B_{dyn} is a 12x4 matrix, K_{inf} is a 4x12 matrix, x is an NHORIZONx12 matrix (where individual columns are accessed here via indexing), d is an NHORIZONx4 matrix, and u is an NHORIZONx4 matrix. A_{dyn} , B_{dyn} , K_{inf} , d and the 0th column of x are inputs, and u is the output. The 1st to (NHORIZON-1)th column of x are intermediate values computed over the course of the benchmark.

This process is repeated until a time horizon, defined as NHORIZON in our code and set to 5 for our evaluations. Note that x is allocated as an (NHORIZON+1)x12 matrix in our code since the unoptimized code accesses up to the (NHORIZON)th column.

Autocomp generates the code in Fig. 25, optimized over several steps from the starting code in Fig. 17. The following optimizations are applied, with the following speedups after each optimization:

1. 1 \times : in this case we treat the unoptimized software as the baseline for speedup, so by definition its speedup is 1 \times .
2. 1.07 \times after “hoist redundant operations out of loops”. Hoists the `mvin` calls for the constant matrices K_{inf} , $Adyn$, and $Bdyn$ above the NHORIZON loop and executes them once rather than in every iteration. Any associated `config_ex` and `config_ld` calls are also moved outside the loop if needed. The `compute` calls use the same scratchpad addresses and may set `B_spad_addr = 0xffffffff` to indicate that the weights are already loaded.
3. 1.13 \times after “loop reordering”. This plan claims to move the configuration and `mvin` instructions for K_{inf} , $Adyn$, and $Bdyn$ before the NHORIZON loop, but this has already been handled in the previous step. In reality, only some configuration instructions that were unnecessarily left behind by the previous step are hoisted.
4. 2.00 \times after “move CPU-based computation to the accelerator”. Replaces CPU-based element-wise negation and addition with equivalent Gemmini compute instructions. Specifically, when x_i and d_i are loaded, a scaling factor of -1 is used to negate it in the scratchpad. The product of K_{inf} and x_i is kept in the accumulator and the negated d_i is multiplied by a dummy 0 vector in order accumulate it on top of this product, enabling data to be kept resident in the accumulator rather than moving it back and forth between the CPU and accelerator memory.
5. 2.12 \times after “hoisting redundant operations out of loops”. Identifies a few `config_ld` instructions that are still redundant and removes them from the loop.
6. 2.66 \times after “loop unrolling”. Changes the outer loop to increment by 2 instead of 1 and duplicate the loop body so each iteration computes two time steps: first $u[i]$ and $x[i+1]$, then $u[i+1]$ and $x[i+2]$. Also merges fence calls at the end of the unrolled loop body if possible. The implementation very aggressively removes fence instructions, which is actually correct as reuse of the same accelerator memory instructions by subsequent `mvin` and `mvout` instructions means that dependencies can be handled internally to the accelerator, rather than via synchronization of both the CPU and accelerator.
7. 2.95 \times after “loop fusion”. Undoes the loop unrolling from the previous step, but keeps the reduced fence instructions. Additionally, this eliminates the unnecessary calculation of $x[NHORIZON]$ during execution, which saves cycles. This optimization makes sense since it is likely the reduced number of fence instructions that improved performance in step 6, rather than the loop unrolling (which usually provides limited benefit, if any).

We further discuss the similarities and differences between the hand-optimized hardware FSM-based implementation in Fig. 24 and the Autocomp-optimized code:

- **Data orchestration.** Due to the coarse-grained nature of the hardware FSM operations and the fact that data movement between the accelerator and main memory is handled within hardware, we are not able to hoist shared data loads of the K_{inf} , $Adyn$, and $Bdyn$ matrices

out of the loop. This is the main advantage the Autocomp-generated software ISA-based implementation has over the hardware FSM-based implementation.

- **Operator fusion.** Both implementations are able to handle all computation on the accelerator, but notably the hardware FSM-based implementation fuses the addition of $d[i]$ into the bias when multiplying K_{inf} and $x[i]$ (then the whole result is negated while storing to main memory), whereas the addition of $d[i]$ is handled as a separate compute instruction in the Autocomp-generated code. So, the hardware FSM-based implementation actually has an advantage in this regard and the Autocomp-generated code has further room for improvement. Both implementations make use of negative scaling of loaded data (via `config_1d` instructions) in order to handle subtraction.
- **Fence instructions.** The Autocomp-generated code is able to remove CPU-based fence instructions and instead handle dependencies within the accelerator, whereas the hardware FSM-based code is forced to place a fence after each matrix multiplication, as accumulated results must be moved back to main memory and loaded to the scratchpad for the next operation.
- **Configuration overhead.** While they do not have as much overhead as fence instructions, configuration instructions can also be blocking. The hand-optimized code hoists configuration instructions out of the loop where possible, but since different matrix sizes must be loaded inside the loop, configuration instructions cannot be completely eliminated, giving Autocomp’s code the advantage in this aspect.
- **Dead code elimination.** Both implementations eliminate the extra computation of $x[NHORIZON]$ that is present in the unoptimized code.

Overall, we find that Autocomp identifies all major optimization opportunities available in the code, with the exception of handling subtraction of $d[i]$ slightly suboptimally. Qualitatively, optimizing this code by hand can be difficult due to a lack of readability and the difficulty of debugging low-level accelerator code. The Autocomp-generated code is well-commented and the sequence of optimizations applied can be easily understood. This will be helpful for further optimization of this benchmark or future optimization of other benchmarks, via methods like the schedule reuse demonstrated in Sec. 5.

C.2.1 Unoptimized Software ISA-Based Code Example

```

void test(float Adyn[12][12], float Bdyn[12][4] float Kinf[4][12], float x[NHORIZON + 1][12][1], float d[
    NHORIZON][4][1], float u[NHORIZON][4][1]) {
    static elem_t Kinf_x[4][1];
    static elem_t A_x[12][1];
    static elem_t B_u[12][1];

    for (int i = 0; i < NHORIZON; i++) {
        // define spad addresses for cached matrices
        // spad is row addressed and each row is 4 elements wide
        static uint32_t A_sp_addr = 0; // 144 elements, 0 to 35
        static uint32_t B_sp_addr = 36; // 48 elements, 36 to 47
        static uint32_t Kinf_sp_addr = 48; // 48 elements, 48 to 59
        static uint32_t C1_sp_addr = 60; // 16 elements, 60 to 63
        static uint32_t C2_sp_addr = 64; // 144 elements, 64 to 99
        static uint32_t x_sp_addr = 100; // 12 elements (at a time), 100 to 111
        static uint32_t u_sp_addr = 112; // 12 elements (at a time), 112 to 123
        static uint32_t acc_start_addr = 1 << 31;

        // tiled_matmul_spad_dram(Kinf, x[i], Kinf_x, NINPUTS, false, false);
        config_ex(WEIGHT_STATIONARY, NO_ACTIVATION, 1, false, false);
        config_st(4, 1.0);
        config_ld(48, 1.000000, 4, 0);
        config_ld(4, 1.000000, 4, 1);
        config_ld(4, 1.000000, 4, 2);
        mvin(Kinf, Kinf_sp_addr, 12, 4);
        mvin2(x[i][0], x_sp_addr, 1, 4);
        preload(x_sp_addr, acc_start_addr, 1, 4, 1, 4);
        compute_preloaded(Kinf_sp_addr, 0xffffffff, 4, 4, 4, 4);
        mvin2(x[i][4], x_sp_addr + 4, 1, 4);
        preload(x_sp_addr + 4, acc_start_addr | (1 << 30), 1, 4, 1, 4);
        compute_preloaded(Kinf_sp_addr + 4, 0xffffffff, 4, 4, 4, 4);
        mvin2(x[i][8], x_sp_addr + 8, 1, 4);
        preload(x_sp_addr + 8, acc_start_addr | (1 << 30), 1, 4, 1, 4);
        compute_preloaded(Kinf_sp_addr + 8, 0xffffffff, 4, 4, 4, 4);
        mvout(Kinf_x[0], acc_start_addr | (1 << 30), 1, 4);
        fence();

        static acc_t Kinf_x_negated[4][1] row_align_acc(1);
        static acc_t d_i_negated[4][1] row_align_acc(1);
        negate_matrix(Kinf_x, Kinf_x_negated, 4, 1);
        negate_matrix(d[i], d_i_negated, 4, 1);
        add_matrix(Kinf_x_negated, d_i_negated, u[i], 4, 1);
    }
}

```

Figure 22: Unoptimized software ISA-based starting code for the TinyMPC primal update forward pass from Sec. 4.5. Achieves 5.7% of theoretical maximum utilization. Continued in Fig. 23.

```

// tiled_matmul_spad_dram(Adyn, x[i], A_x, NSTATES, false, false);
config_ex(WEIGHT_STATIONARY, NO_ACTIVATION, 1, false, false);
config_st(4, 1.0);
config_ld(48, 1.000000, 4, 0);
config_ld(4, 1.000000, 4, 1);
config_ld(4, 1.000000, 4, 2);
for (int chunk = 0; chunk < 3; chunk++) {
    mvin(Adyn[chunk*4], A_sp_addr + chunk*12, 12, 4);
}
mvin2(x[i][0], x_sp_addr, 1, 4);
mvin2(x[i][4], x_sp_addr + 4, 1, 4);
mvin2(x[i][8], x_sp_addr + 8, 1, 4);

preload(x_sp_addr, acc_start_addr, 1, 4, 1, 4);
compute_preloaded(A_sp_addr, 0xffffffff, 4, 4, 4, 4);
preload(0xffffffff, acc_start_addr + 4, 1, 4, 1, 4);
compute_accumulated(A_sp_addr + 12, 0xffffffff, 4, 4, 4, 4);
preload(0xffffffff, acc_start_addr + 8, 1, 4, 1, 4);
compute_accumulated(A_sp_addr + 24, 0xffffffff, 4, 4, 4, 4);

preload(x_sp_addr + 4, acc_start_addr | (1 << 30), 1, 4, 1, 4);
compute_preloaded(A_sp_addr + 4, 0xffffffff, 4, 4, 4, 4);
preload(0xffffffff, (acc_start_addr + 4) | (1 << 30), 1, 4, 1, 4);
compute_accumulated(A_sp_addr + 4 + 12, 0xffffffff, 4, 4, 4, 4);
preload(0xffffffff, (acc_start_addr + 8) | (1 << 30), 1, 4, 1, 4);
compute_accumulated(A_sp_addr + 4 + 24, 0xffffffff, 4, 4, 4, 4);

preload(x_sp_addr + 8, acc_start_addr | (1 << 30), 1, 4, 1, 4);
compute_preloaded(A_sp_addr + 8, 0xffffffff, 4, 4, 4, 4);
preload(0xffffffff, (acc_start_addr + 4) | (1 << 30), 1, 4, 1, 4);
compute_accumulated(A_sp_addr + 8 + 12, 0xffffffff, 4, 4, 4, 4);
preload(0xffffffff, (acc_start_addr + 8) | (1 << 30), 1, 4, 1, 4);
compute_accumulated(A_sp_addr + 8 + 24, 0xffffffff, 4, 4, 4, 4);

mvout(A_x[0], acc_start_addr, 1, 4);
mvout(A_x[4], acc_start_addr + 4, 1, 4);
mvout(A_x[8], acc_start_addr + 8, 1, 4);
fence();

// tiled_matmul_spad_dram(Bdyn, u[i], B_u, NSTATES, false, false);
config_ex(WEIGHT_STATIONARY, NO_ACTIVATION, 1, false, false);
config_st(4, 1.0);
config_ld(16, 1.000000, 4, 0);
config_ld(4, 1.000000, 4, 1);
config_ld(4, 1.000000, 4, 2);
for (int chunk = 0; chunk < 3; chunk++) {
    mvin(Bdyn[chunk*4], B_sp_addr + chunk*4, 4, 4);
}
mvin2(u[i][0], x_sp_addr, 1, 4);
preload(x_sp_addr, acc_start_addr, 1, 4, 1, 4);
compute_preloaded(B_sp_addr, 0xffffffff, 4, 4, 4, 4);
preload(0xffffffff, acc_start_addr + 4, 1, 4, 1, 4);
compute_accumulated(B_sp_addr + 4, 0xffffffff, 4, 4, 4, 4);
preload(0xffffffff, acc_start_addr + 8, 1, 4, 1, 4);
compute_accumulated(B_sp_addr + 8, 0xffffffff, 4, 4, 4, 4);
mvout(B_u[0], acc_start_addr, 1, 4);
mvout(B_u[4], acc_start_addr + 4, 1, 4);
mvout(B_u[8], acc_start_addr + 8, 1, 4);
fence();

add_matrix(A_x, B_u, x[i+1], 12, 1);
}
}

```

Figure 23: Unoptimized software ISA-based starting code for the TinyMPC primal update forward pass, continued from Fig. 22.

C.2.2 Optimized Hardware FSM-Based Code Example

```

void test(float Adyn[12][12], float Bdyn[12][4] float Kinf[4][12], float x[NHORIZON + 1][12][1], float d[
    NHORIZON][4][1], float u[NHORIZON][4][1]) {
    static elem_t B_u[12][1];

    gemmini_extended_config_ex(1, 0, 0, 1, false, false);
    gemmini_extended3_config_ld(4, 1.0, false, 1);
    gemmini_extended3_config_ld(4, 1.0, false, 2);
    for (int i = 0; i < NHORIZON; i++) {
        gemmini_extended_config_st(4, 0, -1.0);
        gemmini_extended3_config_ld(48, 1.0, false, 0);
        gemmini_loop_ws(1, 1, 3, 0, 3, 0, Kinf, x[i], d[i], u[i], 12, 1, 1, 1, false, false, false,
            true, 0, 1, 1, false);
        gemmini_fence();

        if (i < NHORIZON - 1) {
            gemmini_extended_config_st(4, 0, 1.0);
            gemmini_extended3_config_ld(16, 1.0, false, 0);
            gemmini_loop_ws(3, 1, 1, 0, 3, 0, Bdyn, u[i], NULL, B_u, 4, 1, 1, 1, false, false, false,
                false, 0, 1, 1, false);
            gemmini_fence();

            gemmini_extended3_config_ld(48, 1.0, false, 0);
            gemmini_loop_ws(3, 1, 3, 0, 3, 0, Adyn, x[i], B_u, x[i+1], 12, 1, 1, 1, false, false, false,
                true, 0, 1, 1, false);
            gemmini_fence();
        }
    }
}

```

Figure 24: Example of the TinyMPC primal update forward pass from Fig. 22, hand-optimized and using the hardware FSM, from the experiments. Achieves 10.9% of theoretical maximum utilization.

C.2.3 Autocomp-Generated Code Example

```

void test(float Adyn[12][12],
        float Bdyn[12][4],
        float Kinf[4][12],
        float x[NHORIZON + 1][12][1],
        float d[NHORIZON][4][1],
        float u[NHORIZON][4][1]) {

    // Define scratchpad addresses for all matrices.
    uint32_t A_sp_addr      = 0;
    uint32_t B_sp_addr      = 36;
    uint32_t Kinf_sp_addr   = 48;
    uint32_t x_sp_addr      = 100;
    uint32_t acc_start_addr = 1 << 31; // MSB = 1 indicates accumulator address

    //-----
    // Hoisted Invariant Matrix Loads: These matrices do not change over
    // the horizon. We load them once into the Gemmini scratchpad.
    //-----
    config_ex(WEIGHT_STATIONARY, NO_ACTIVATION, 1, false, false);
    config_st(4, 1.0);

    // Load constant weight matrix Kinf.
    config_ld(48, 1.000000, 4, 0);
    mvin(Kinf, Kinf_sp_addr, 12, 4);

    // Load constant system dynamics matrix Adyn.
    config_ld(48, 1.000000, 4, 0);
    for (int chunk = 0; chunk < 3; chunk++) {
        mvin(Adyn[chunk * 4], A_sp_addr + chunk * 12, 12, 4);
    }

    // Load constant control dynamics matrix Bdyn.
    config_ld(16, 1.000000, 4, 0);
    for (int chunk = 0; chunk < 3; chunk++) {
        mvin(Bdyn[chunk * 4], B_sp_addr + chunk * 4, 4, 4);
    }
}

```

Figure 25: Example of an Autocomp-optimized version of the TinyMPC primal update forward pass from Fig. 22. Achieves 15.7% of theoretical maximum compute utilization. Continued in Fig. 26.

```

-----  

// Outer horizon loop with fusion of iterations and operations.  

-----  

for (int i = 0; i < NHORIZON; i++) {  

    // Compute u[i] = -(kinf*x[i]) - d[i]  

    config_ld(4, -1.000000, 4, 1);  

    mvin2(x[i][0], x_sp_addr, 1, 4);  

    preload(x_sp_addr, acc_start_addr, 1, 4, 1, 4);  

    compute_preloaded(Kinf_sp_addr, 0xffffffff, 4, 4, 4, 4);  

    mvin2(x[i][4], x_sp_addr + 4, 1, 4);  

    preload(x_sp_addr + 4, acc_start_addr | (1 << 30), 1, 4, 1, 4);  

    compute_preloaded(Kinf_sp_addr + 4, 0xffffffff, 4, 4, 4, 4);  

    mvin2(x[i][8], x_sp_addr + 8, 1, 4);  

    preload(x_sp_addr + 8, acc_start_addr | (1 << 30), 1, 4, 1, 4);  

    compute_preloaded(Kinf_sp_addr + 8, 0xffffffff, 4, 4, 4, 4);  

    mvin2(d[i], x_sp_addr, 1, 4);  

    config_ld(4, 1.000000, 4, 1);  

    mvin2(0, x_sp_addr + 4, 1, 4);  

    preload(x_sp_addr + 4, acc_start_addr | (1 << 30), 1, 4, 1, 4);  

    compute_accumulated(x_sp_addr + 4, x_sp_addr, 1, 4, 1, 4);  

    mvout(u[i], acc_start_addr, 1, 4);  

    if (i < NHORIZON - 1) {  

        // Compute A_x = Adyn * x[i]  

        mvin2(x[i][0], x_sp_addr, 1, 4);  

        mvin2(x[i][4], x_sp_addr + 4, 1, 4);  

        mvin2(x[i][8], x_sp_addr + 8, 1, 4);  

        preload(x_sp_addr, acc_start_addr, 1, 4, 1, 4);  

        compute_preloaded(A_sp_addr, 0xffffffff, 4, 4, 4, 4);  

        preload(0xffffffff, acc_start_addr + 4, 1, 4, 1, 4);  

        compute_accumulated(A_sp_addr + 12, 0xffffffff, 4, 4, 4, 4);  

        preload(0xffffffff, acc_start_addr + 8, 1, 4, 1, 4);  

        compute_accumulated(A_sp_addr + 24, 0xffffffff, 4, 4, 4, 4);  

        preload(x_sp_addr + 4, acc_start_addr | (1 << 30), 1, 4, 1, 4);  

        compute_preloaded(A_sp_addr + 4, 0xffffffff, 4, 4, 4, 4);  

        preload(0xffffffff, (acc_start_addr + 4) | (1 << 30), 1, 4, 1, 4);  

        compute_accumulated(A_sp_addr + 4 + 12, 0xffffffff, 4, 4, 4, 4);  

        preload(0xffffffff, (acc_start_addr + 8) | (1 << 30), 1, 4, 1, 4);  

        compute_accumulated(A_sp_addr + 4 + 24, 0xffffffff, 4, 4, 4, 4);  

        preload(x_sp_addr + 8, acc_start_addr | (1 << 30), 1, 4, 1, 4);  

        compute_preloaded(A_sp_addr + 8, 0xffffffff, 4, 4, 4, 4);  

        preload(0xffffffff, (acc_start_addr + 4) | (1 << 30), 1, 4, 1, 4);  

        compute_accumulated(A_sp_addr + 8 + 12, 0xffffffff, 4, 4, 4, 4);  

        preload(0xffffffff, (acc_start_addr + 8) | (1 << 30), 1, 4, 1, 4);  

        compute_accumulated(A_sp_addr + 8 + 24, 0xffffffff, 4, 4, 4, 4);  

        // Compute B_u = Bdyn * u[i] and accumulate onto A_x  

        mvin2(u[i][0], x_sp_addr, 1, 4);  

        preload(x_sp_addr, acc_start_addr | (1 << 30), 1, 4, 1, 4);  

        compute_preloaded(B_sp_addr, 0xffffffff, 4, 4, 4, 4);  

        preload(0xffffffff, (acc_start_addr + 4) | (1 << 30), 1, 4, 1, 4);  

        compute_accumulated(B_sp_addr + 4, 0xffffffff, 4, 4, 4, 4);  

        preload(0xffffffff, (acc_start_addr + 8) | (1 << 30), 1, 4, 1, 4);  

        compute_accumulated(B_sp_addr + 8, 0xffffffff, 4, 4, 4, 4);  

        mvout(x[i + 1][0], acc_start_addr, 1, 4);  

        mvout(x[i + 1][4], acc_start_addr + 4, 1, 4);  

        mvout(x[i + 1][8], acc_start_addr + 8, 1, 4);  

        fence();  

    }  

}
}

```

Figure 26: Example from Fig. 25, continued.